LARGE SCALE MODEL EXPERIMENTS OF RECYCLED BASE COURSE MATERIALS STABILIZED WITH CEMENT AND CEMENT KILN DUST

by

Brian R. Kootstra

A thesis submitted in partial fulfillment
of the requirements for the degree of

MASTER OF SCIENCE

CIVIL AND ENVIRONMENTAL ENGINEERING

at the

UNIVERSITY OF WISCONSIN-MADISON

Spring 2009

EXECUTIVE SUMMARY

The objectives of this study were to determine the resilient modulus of two recycled roadway materials: recycled pavement material (RPM) and road surface gravel (RSG) with and without cement and cement kiln dust (CKD) stabilization. The resilient modulus was determined by conducting Large Scale Model Experiments (LSME) designed to replicate field conditions, and compared with the resilient modulus determined from the laboratory test method described by NCHRP 1-28A. Results of wet-dry and freeze-thaw durability tests were used to select a portland cement content of 4% by weight and a CKD content of 10% by weight to chemically stabilize RPM and RSG. The stiffness at curing times of 7 and 28 days was evaluated, and the summary resilient modulus (SM_R) corresponding to a bulk stress of 208 kPa was used to calculate AASHTO base layer coefficients for use in pavement layer thickness design. A conventional base course material specified as a Class 5 material gradation employed in Minnesota, and similar to AASHTO grading C, was used as a reference material.

Durability test results indicated that RPM and RSG blended with cement were much more durable than when blended with CKD based on the percent mass loss. Freeze-thaw cycling resulted in greater mass loss than wet-dry cycling. Significant expansion of the test specimens blended with CKD was observed, which could cause damage to pavement structures.

Both RPM and RSG had plastic deformations greater than Class 5 base. The addition of either cement or CKD significantly reduced both plastic deformations and elastic deflections measured in the LSME. The greatest plastic deformations measured in the LSME were for unstabilized RSG; however, RSG blended with 10% CKD resulted in the least plastic deformation.

The modulus of RPM and RSG increased significantly with the addition of cement and CKD. Unstabilized RSG had the largest elastic deflections, resulting in the lowest

resilient modulus (120 MPa for a 0.20 m layer thickness and 220 MPa for a 0.30 m layer thickness) and RSG blended with CKD at 28 days of curing had the highest resilient modulus (1340 MPa). For 0.30 m thick layers, the modulus of RPM with 4% cement after 28 days of curing was 2.4 times higher than unstabilized RPM, while RPM with 10% CKD was 2.1 times greater. The modulus of RSG with cement increased by a factor of 4.6 compared to unstabilized RSG, and by a factor of 6.1 for RSG with CKD. The stabilized base materials continued to increase in stiffness between curing times of 7 and 28 days, with the exception of RPM blended with cement. RPM and RSG blended with CKD gained greater stiffness compared to cement, although the cement stabilization resulted in a higher 7 day modulus.

The summary moduli determined from the LSME tests with stabilized materials were much less than the summary moduli measured in the laboratory resilient modulus tests with internal LVDTS, but greater than that determined with external LVDTs. Differences in mixing of the recycled materials with cement and CKD and curing conditions may also contribute to the difference in the modulus between the laboratory and LSME. The LSME modulus is expected to be closer to actual field conditions than the laboratory test.

Unstabilized RPM had a modulus slightly greater than Class 5 base for each thickness evaluated. The modulus increased with increasing base layer thickness for all three unstabilized materials due to the strain dependency of modulus of granular materials. The resilient modulus was found to increase with the bulk stress for the unstabilized granular base course materials indicating the nonlinearity of these soils. However, with the addition of cement and CKD, the resilient modulus did not show stress dependency for a range of stresses typically resulting from wheel loads and these materials were considered to be linear elastic.

AASHTO layer coefficients were calculated from the resilient modulus determined in the LSME for use in pavement thickness design. The layer coefficients for the unstabilized materials increased with layer thickness, reflecting the increase in modulus with a thicker layer. Layer coefficients for RPM and RSG blended with cement and CKD remain constant with layer thickness, and are greater than unstabilized layer coefficients, indicating increased structural capabilities.

This study has shown that the addition of cement or CKD can significantly improve the stiffness of RPM and RSG, having the potential to allow greater use of recycled roadway materials in the reconstruction of roads, minimizing construction costs and environmental impacts. However, the low durability of materials mixed with CKD should be investigated further, because the expansion may be damaging to pavement structures.

ACKNOWLEDGEMENT

First and foremost, I would like to thank my advisor, Professor Tuncer Edil for his support, advice and guidance through this study and other research during my graduate studies at the University of Wisconsin-Madison. I sincerely thank Professors James Tinjum and Hussain U. Bahia for participating as thesis defense committee members, and to Professors Craig H. Benson and Dante Fratta for valuable guidance and support on several aspects of this work. I would also like to thank the Portland Cement Association Education Foundation for awarding me the fellowship to conduct this research.

I would like to thank Xiaodong Wang and Bill Lang for their continual support and assistance throughout this research. I acknowledge the help and support of many GeoEngineering students past and present including: Ali Ebrahimi, Felipe Camargo, Craig Schuettpelz, Dr. Young Hwan Son, Jeremy Baugh, Greg Schaertl and Alex Boecher. Whether participating on a project together, discussing research, or just providing support, each person deserves recognition and has made important contributions to the department's great atmosphere.

Thank you to Raymond C. McVeigh and the Lafarge Cement Company for donating the CKD used in this study.

Finally and most sincerely, I thank my wife, Sarah, for her continual support and encouragement.

TABLE OF CONTENTS

LIST OF FIGURES

LIST OF TABLES

1. INTRODUCTION

There are approximately 4.0 million miles of public roads in the United States requiring billions of dollars and significant amounts of natural resources to maintain each year. There are also over 1.6 million miles of unpaved gravel roads in the United States. Increased development, leading to increases in traffic and vehicle loads, has put significant pressure on local governments to upgrade and pave these roads at considerable expense. The ability to reuse the materials comprising these existing roads, such as deteriorated asphalt concrete and underlying base course generally consisting of coarse aggregate or road surface gravel in unpaved roads, would provide an attractive alternative to using additional natural resources providing economic and environmental benefits. There is a strong interest in developing effective, convenient and economic methods to upgrade and reconstruct these roads.

During the process of reconstructing a deteriorated paved road or gravel road, a large supply of potentially useful materials would be conveniently located along the existing roadway, leading to significant time and cost savings relative to conventional total reconstruction costs. These cost savings would result from less time and expense spent on transportation and procurement of new materials and the disposal of the old material. Instead of disposing deteriorated roadway materials in a landfill, the existing surface pavement can be pulverized and mixed with the underlying base course and placed directly into the road as a new base course in a process known as full depth reclamation, relieving pressure on natural aggregate resources. Similarly, road surface gravel can be used as a new base. The technology should be particularly useful to smaller communities and rural counties without large construction budgets.

Recycled pavement material (RPM) and road surface gravel (RSG) are two materials that can be reused as new base course in the rehabilitation of roads (Wen et

al. 2004; Li et al. 2008; Hatipoglu et al. 2008). RPM is a mixture of crushed deteriorated asphalt pavement and the underlying base course material. This material can be created in situ and then a new layer of hot mix asphalt is placed over the RPM. The riding surface of most unpaved roads consists of RSG. The RSG in these roads can also be recycled by forming a base for asphalt pavement.

Since RPM and RSG may not perform as well as natural high quality aggregates relative to strength, stiffness and rutting potential, the addition of a stabilizing material such as cement or cement kiln dust (CKD) can improve these properties due to cementation. CKD is an industrial byproduct consisting of leftover materials from the manufacturing of portland cement. The use of CKD as a binder may be less expensive as compared to portland cement, while creating a use for an industrial byproduct that is often disposed of in landfills (Todres et al. 1992).

The particular objectives of this study were to determine the resilient modulus of RPM and RSG with and without CKD and cement stabilization in a Large Scale Model Experiment (LSME) designed to replicate field conditions, and to determine AASHTO structural layer coefficients of the tested materials for use in pavement thickness design. Summary resilient moduli for use in the new Mechanistic-Empirical Design of highway pavements are also determined. This thesis describes the findings of this study. A background in Section 2 highlights results of related studies. Materials and methods are described in Sections 3 and 4. Results and analysis are provided in Section 5, and a summary and conclusions are in Section 6.

2. BACKGROUND

2.1. RECYCLING OF ROADWAY MATERIALS

Maintenance of existing roads is constantly required due to deterioration of the pavement structure resulting from traffic loading and the effect of the local environmental conditions. The ability to recycle existing pavement materials in the rehabilitation and reconstruction of roads provides an attractive alternative to other methods such as the full removal and replacement of the pavement materials. An in-situ recycling process known as full-depth reclamation (FDR) can be employed with deteriorated asphalt pavements, where the existing asphalt surface layers are pulverized and mixed with the underlying aggregate base and/or subgrade, forming a recycled base layer commonly called RPM, on which a new asphalt surface layer is placed. The depth of pulverization typically ranges from 100 to 300 mm (4 to 12 in), which may include part of the underlying subgrade soils (Epps 1990), but may also involve less than the full depth of pavement materials. Cases in which FDR may be the best solution include the reconstruction of highly deteriorated pavements where a simple overlay cannot be placed, or pavements where the distresses indicate deficiencies in the base or subgrade.

FDR can also be used to upgrade an unpaved road with an aggregate surface to an asphalt surface, where the road surface gravel such as the RSG used in this study, is mixed with a stabilizing material and compacted forming the base course for the asphalt pavement (Hatipoglu et al. 2008).

Recycling pavement materials using FDR is both cost effective and environmentally friendly. One of the major advantages of implementing FDR is the cost savings as compared to a full removal and replacement, which are normally 25% to 50% less (Luhr 2005). These cost savings are a result of not having to purchase and transport valuable

virgin aggregate resources, while at the same time reducing the amount of waste from the deteriorated roadway that may otherwise have to be disposed of. Additional environmental benefits include conservation of energy, the reduction of greenhouse gasses, and reducing materials disposed of in landfills (Kearney and Huffman 1999; Wen and Edil 2009).

2.2. STABILIZATION OF RECYCLED ROADWAY MATERIALS

An increasing amount of asphalt binder or recycled asphalt pavement (RAP) content in a mixture of recycled pavement materials may adversely affect strength, stiffness and plastic strains (Taha et al. 1999; Cooley 2005; Kim et al. 2007; Camargo 2009). A common method to increase the strength, stiffness and durability of these materials is to mix in one or more stabilizing agents such as cement, asphalt emulsions, lime, cement kiln dust (CKD), or fly ash.

2.2.1. Recycled Materials Blended with Cement.

Cement is often added to the mixture of pulverized asphalt and aggregate materials to increase strength and durability, and methods of design and construction are described in the Portland Cement Association's Guide to Cement Treated Base (Halsted et al. 2006). This publication gives typical properties of CTB including compressive strength ranging from 2.1 – 5.5 MPa (300 – 800 psi) and modulus of elasticity from 4,100 – 6,900 MPa (600,000 to 1,000,000 psi). Guthrie et al. (2007) determined that the optimum cement content for a mixture of 50% reclaimed asphalt pavement (RAP) and 50% base materials was 1.0% based on results of unconfined compressive strength (UCS) tests and tube suction tests. Mallick et al. (2002) reported increases in strength and stiffness of an FDR material mixed with 5% cement along with other types of additives.

2.2.2. Recycled Materials Blended with Cement Kiln Dust (CKD).

CKD is an industrial byproduct resulting from the production of portland cement, and is collected by fabric filters or electrostatic precipitators. CKD is a mixture of partially calcined and unreacted raw feed, clinker dust and ash enriched with sulfates, halides, and other volatiles. The chemical and physical properties of CKD vary widely and depend on factors such as raw materials used in production and the manufacturing process. CKD with a low loss on ignition (LOI) and a high CaO content has been used most effectively to stabilize soils for base and subbase applications, usually in combination with other stabilizing materials such as cement or fly ash (Adaska and Taubert 2008).

The effect of blending CKD with mixtures of recycled asphalt pavement (RAP) and virgin aggregate was investigated by Taha (2003) by performing UCS tests. Various percentages of CKD ranging from 0% to 20% were blended with the following RAP-virgin aggregate mixtures: 100%-0%, 90%-10%, 80%-20%, 0%-100%. Compaction tests were performed at modified Proctor compactive effort, where the maximum dry unit weight was found to increase with increasing CKD and virgin aggregate content. The optimum moisture content increased with increasing aggregate content and also with increasing CKD contents up to 7%; however, optimum moisture content decreased with CKD contents of 10% or greater. UCS test results indicated that strength increased with increasing virgin aggregate, and that a significant strength gain took place between 7 and 28 days of curing. 15% CKD content demonstrated the highest strength gain.

Baugh (2008) studied the effects of blending CKD with several recycled roadway materials including RAP, RPM and RSG. The RAP consisted entirely of milled asphalt, whereas the RPM had a limestone base course mixed in. CKD contents of 5%, 10%, 15%, and 20% were evaluated with standard compaction, CBR, resilient modulus and

unconfined compressive strength testing. The maximum dry unit weight was found to decrease and the optimum moisture content increased with increasing CKD content. After 7 days of curing, the CBR of materials with CKD increased 6 to 9 times over untreated material. The resilient modulus increased 75 to 650% after 56 days of curing, but no trend was identified for increasing CKD content. The UCS testing showed increasing strength with greater curing time and CKD content.

Although little other published work is available on the topic of blending CKD with recycled pavement materials, research showing promising results of blending CKD with both granular and fine-grained soils has been accomplished.

CKD improves engineering properties such as strength and stiffness of sandy soils due to the pozzolanic reactions that take place (Bhatty et al. 1996). Soil particles are cemented together due to the reaction of silica and hydrated lime that forms calcium silicate hydrite. Several engineering properties of a dune sand blended with various amounts of CKD were investigated by Baghdadi et al. (1995). In preparation for UCS tests, specimens were created with CKD contents of 10%, 20%, 50%, 75% and 100% and cured for 7, 28 and 90 days. Compaction of the specimens was performed at 100% of maximum dry unit weight and optimum water content. Additional testing was performed on specimens having strength results satisfactory for road subbases, including durability, CBR and split tension. Results of UCS tests showed increasing strength with increasing CKD content. UCS specimens of 50% and 100% CKD were tested both unsoaked and after a 24 hour period of soaking, where the soaked strength was found to be about 15% less than the unsoaked specimens. Sand blended with 12% to 50% CKD was reported satisfactory for road construction. Although specimens of 75% and 100% CKD had high compressive strengths, they failed the durability requirements.

Zaman et al. (1999) investigated the effects on resilient modulus, unconfined compressive strength and durability of crushed limestone blended with CKD. The resilient modulus increased a maximum of 73% with the addition of 15% CKD. Durability was investigated by subjecting specimens to freeze-thaw and wet-dry cycles. A reduction of the resilient modulus by 68% was observed after 8 freeze-thaw cycles, while a 62% reduction was observed for 12 wet-dry cycles. The UCS was shown to decrease over either 4 wet-dry or freeze-thaw cycles, after which no additional decrease was seen.

2.3. RESILIENT MODULUS

Pavement design methods are continuing to become more analytical, or mechanistic, so they can be applied accurately to a variety of design scenarios, as opposed to empirical methods determined from observations or experience with certain materials, locations, etc. Resilient modulus (M_R) is an important engineering property used in mechanistic-empirical pavement design, and is a measure of the stiffness of pavement materials. M_R of base and subbase materials is a key input into the mechanistic-empirical pavement design procedure, where an incorrect input will cause inaccurate predictions of pavement response and performance (NCHRP 2004). The resilient modulus of HMA, base, subbase and subgrade can be determined by laboratory or in-situ testing.

2.3.1. Definition of Resilient Modulus.

Resilient modulus can be defined as the elastic modulus based on the recoverable strain under repeated loads (Huang 2004), or mathematically as:

$$M_R = \frac{\sigma_d}{\varepsilon_r} \tag{2.1}$$

where σ_d is the deviator stress and ε_r is the resilient strain. The resilient modulus defined by Eqn. 2.1 is equivalent to Young's modulus of a completely linear elastic material. A completely linear elastic material deforms under a cyclic load, and then returns to its original dimensions after unloading. Typical base and subbase materials are not completely elastic, because some permanent deformation occurs during each load application, resulting in non-recoverable plastic strain (Mitchell 1993). The strain that is recovered during each loading cycle is known as the resilient or elastic strain.

The resilient portion of the strain can be used to evaluate non-linear elastic pavement materials after repetitive loading if the load is small compared to the strength of the material. During cyclic loading tests of soils, Muhanna et al. (1998) found that over half of the total cumulative permanent deformation occurred in the first 10 loading cycles. The amount of plastic deformation approaches zero with increasing loading cycles, while the elastic strain becomes constant. Therefore, the resilient modulus should be determined based on linear elastic behavior that occurs after a number of loading cycles have taken place.

2.3.2. Factors Affecting the Resilient Modulus of Pavement Materials.

Several factors affect the resilient modulus of granular pavement materials, with stress level having the most significant impact (Hicks 1970; Kolisoja 1997). The resilient modulus increases significantly with an increase in confining pressure or the bulk stress, which is the sum of the three principal stresses. The resilient modulus of granular materials is also affected by strain amplitude (Seed and Idriss 1970; Hardin and Drnevich 1972; Edil and Luh 1978), resulting in resilient modulus being sensitive to the thickness of the layer being evaluated due to varying strain levels within the layer (i.e. thicker layers have a higher elastic modulus at a given bulk stress).

Several studies have shown that as the density of granular materials increases the resilient modulus also increases (Rada and Witczak 1981; Kolisoja 1997). With greater compaction and density, the number of inter-particle contacts increase, decreasing the average contact stress resulting from a load, causing a decrease in deformation and an increase in the resilient modulus. Water content also affects the resilient modulus, where a decrease in the resilient modulus occurs with increasing water content, especially above optimum (Hicks and Monismith 1971). For example, Haynes and Yoder (1963) reported a 50% decrease in the resilient modulus of a gravel when the degree of saturation was increased from 70% to 97%. When granular materials become saturated, excess pore-water develops under cyclic loading, causing a decrease in the effective stress, which in turn causes a decrease in strength and stiffness.

Research has shown that the stiffness of granular materials also depends on grain size distribution, fines content, and particle shape. The resilient modulus has been shown to increase with increasing maximum particle size for materials with similar grain size distribution, shape and fines content (Thom 1988; Kolisoja 1997). Particle size distribution has been shown to have a minor impact, although well-graded soils tend to have a higher resilient modulus than uniformly graded soils, due to more densely packed particles in the well-graded material. Generally, researchers have reported a decrease in resilient modulus with increasing fines content (Thom and Brown 1987; Kamal et al. 1993), although results have varied depending on the type of soils and if the fines were low-plasticity or high-plasticity. Most research has shown that materials with more angular to subangular particles will have a higher resilient modulus due to better load spreading capabilities than that of subrounded or rounded particles (Hicks and Monismith, 1971; Thom 1988).

Factors that have little effect on the resilient modulus of granular materials include the loading duration, frequency and sequence (Seed et al. 1965; Hicks 1970).

2.3.3. Determination of the Resilient Modulus of Pavement Materials.

The resilient modulus of soils varies with the state of stress, which can be defined by the confining pressure and the cyclic load, or deviator stress. Common laboratory tests apply a range of confining pressures and deviator stresses to a specimen, and specific combinations of these stresses have been standardized by AASHTO and NCHRP, reflecting loading situations typical of soils in pavement structures.

A power model first proposed by Moosazedh and Witczak (1981) commonly used to describe the constitutive relationship between the resilient modulus and state of stress of granular materials is presented as Eqn. 2.2,

$$M_R = k_1\left(\frac{\theta}{p_o}\right)^{k_2} \tag{2.2}$$

where θ is the bulk stress, p_o is a reference stress (1 kPa), and k_1 and k_2 are empirically fitted constants that are unique for a given material. Finn et al. (1986) reported that with a k_2 of 0.6 and k_1 ranging from 3200 to 8000 psi, the base and subbase materials used in the AASHO road test could be described with Eqn. 2.2. The bulk stress is the sum of the three principal stresses (σ_1, σ_2 and σ_3),

$$\theta = \sigma_1 + \sigma_2 + \sigma_3 \tag{2.3}$$

which includes the stress from cyclic loading along with the geostatic stress resulting from the weight of the overlying pavement layers.

2.3.4. Use of Large Scale Model Experiments to Determine Resilient Modulus.

Tanyu et al. (2003) used a large scale model experiment (LSME) to determine the resilient modulus of granular pavement materials used for bases and subbases. The LSME is a large prototype-scale test apparatus that simulates an actual pavement test section, and provides a means of determining resilient modulus that is more

representative of actual wheel loads applied to pavement structures in the field compared to typical laboratory tests. The resilient modulus is backcalculated from loads and deflections measured in the LSME. A base and riding surface layer were not included in the LSME; however, the load applied to the subbase surface was reduced to account for the stress reduction caused by these materials. Results indicated that the resilient modulus of granular materials obtained from conventional laboratory tests tend to be lower than results calculated from the LSME. For gravels used as subbases this difference was small, while significantly higher for a sand-like industrial byproduct. These differences were assumed to be due to the state of stress, strain level, number of loading cycles, and scale. The resilient modulus measured in the LSME was also sensitive to thickness, where thicker layers had a higher resilient modulus primarily due to reduced strain level for the same loading (Tanyu et al. 2003).

The LSME has also been used to determine equivalency criterion for granular working platform materials based on measured deflections (Tanyu et al. 2004).

3. MATERIALS

3.1. BASE MATERIALS

The three base materials selected for this study consisted of a conventional aggregate base material, recycled pavement material (RPM), and road surface gravel (RSG). RPM and RSG are recycled materials. The conventional base was used as a reference material.

The conventional base material is referred to as Class 5 gravel, because it meets the Minnesota Department of Transportation (MnDOT) gradation specifications for Class 5 base course (MnDOT 2005). Class 5 base is similar to the crushed gravel Gradation No. 2 per the Wisconsin Department of Transportation specification P-208 for aggregate base course and AASHTO Grading C as described by AASHTO M 147 (AASHTO 2001). The particle size distribution for the Class 5 used in this study is shown in Fig. 3.1(a) along with the upper and lower boundaries of the MnDOT specification. The Class 5 gravel was created by combining a pit run sand obtained from Wimme Sand and Gravel (Plover, Wisconsin) with crushed pea gravel from Midwest Decorative Stone and Landscape Supply (Madison, WI). The pit run was screened using a 25 mm sieve before adding the pea gravel (Camargo 2008).

The RPM was obtained from a road reconstruction project near the intersection of Muir Field Road and Carnwood Road in southwestern Madison, WI. The RPM consisted of approximately equal fractions of pulverized hot mix asphalt and limestone base course from the roadway that was being reconstructed (Camargo 2008).

The RSG material was created by combining the previously made Class 5 gravel with fine-grained soil obtained from Rosenbaum Crushing and Excavating (Stoughton, Wisconsin) so that the combined material met the gradation and plasticity requirements for surface course materials that are described in AASHTO M 147 (AASHTO 2001). The

particle size distribution of the RSG is shown if Fig. 3.1(b) along with the AASHTO limits for three types of surface course gravel stipulated as D, E, and F. The RSG used for this study contained plastic fines resulting in the soil displaying some plasticity with 3% of the particle diameters less than the 2 micron clay fraction.

A summary of index properties and soil classifications for the three base materials is shown in Table 3.1. The Class 5 gravel classifies as SP, RPM as GW-GM, and RSG as SC-SM in the Unified Soil Classification System described in ASTM D 2487. In the AASHTO Soil Classification System (ASTM D 3282) Class 5 gravel and RPM classify as A-1-a and RSG as A-2-4. Class 5 and RPM are both non-plastic, while the RSG had a liquid limit (LL) of 21 and a plasticity index (PI) of 7. The particle size distribution curves of the materials, determined using ASTM D 422, are shown together in Fig. 3.2.

Compaction tests on each material were performed at standard compactive effort (ASTM D 698). The compaction curves are shown in Fig 3.3. Optimum water contents and maximum dry unit weights for the base materials with and without stabilizing materials are summarized in Table 3.2. For nearly all cases, the addition of the CKD or cement increases the optimum water content and decreases the maximum dry unit weight. The compaction curve for Class 5 gravel shows that the dry unit weight of this material is insensitive to water content, whereas the bell shaped curves obtained for the RPM and RSG show that the maximum dry unit weight is sensitive to the water content (Fig. 3.3).

3.2. CEMENT AND CEMENT KILN DUST (CKD)

Type 1 portland cement was used as a means of stabilizing the RPM and RSG. The cement was purchased locally in 42.6 kg (94 lb) sacks manufactured by Quikrete®.

CKD was obtained from the Lafarge cement plant in Alpena, MI. The Alpena plant produces cement from limestone, silica, alumina and iron which is ground into a raw mix that is fed into rotary kilns and heated to 1480 °C (2700 °F). A chemical analysis of the CKD provided by the manufacturer is presented in Table 3.3, along with typical chemical compositions of CKD found in the literature, which vary widely due to the type of manufacturing process and raw materials used. The chemical composition of Alpena CKD is primarily within the bounds found in the literature, except for higher amounts of free lime (CaO) and sulfur trioxide (SO_3), and a lower loss on ignition (LOI). Table 3.3 also includes the CKD chemical composition reported by Baugh (2008) whose results are summarized in Section 2.2.2.

4. METHODS

4.1. LARGE SCALE MODEL EXPERIMENT

4.1.1. Apparatus and Loading Methodology

The large scale model experiment (LSME) is a test apparatus for evaluating deflections during cyclic loading of a prototype-scale pavement structure (or parts of it) in a manner that replicates field conditions as closely as practical (Tanyu et al 2003). A schematic of the LSME is shown in Fig. 4.1. The LSME consists of a pavement profile constructed in a 3 m x 3 m x 3 m test pit. A loading frame, actuator (280 L/m MTS hydraulic actuator with 100 kN capacity and 168 mm stroke), and steel loading plate (125 mm radius, 25 mm thickness) are used to apply loads simulating those applied by vehicles. Loads are applied with a load pulse consisting of a 0.1 s loading period followed by a 0.9 s rest period. The load (L) varies temporally as a haversine function. With t=0 at the peak, the load function is expressed as:

$$L(t) = q \sin^2\left(\frac{\pi}{2} + \frac{\pi t}{d}\right) \tag{4.1}$$

where q is the maximum load, d is the duration of load, and t is time. All pavement profiles in the LSME were subjected to 10,000 cycles of traffic wheel loads simulating 4-axle trucks (70 kN per axle and 35 kN per wheel set) with a tire pressure of 700 kPa and a circular contact area with radius of 125 mm.

The pavement profile consisted of a 2.5-m-thick bottom layer of uniform sand simulating a deep and stiff subgrade overlain by a base course layer comprised of the materials being evaluated (Class 5 gravel, RPM, RSG, and stabilized mixtures). An asphalt surface layer was not included. The stress to be applied at the surface of the base course was estimated by conducting nonlinear finite-element analyses of the pavement profile with the program MICH-PAVE (Harichandran et al. 1989), which is

described in Appendix B. The asphalt surface was assumed to have an elastic modulus of 3540 MPa, a Poisson's ratio (ν) of 0.35 (Huang, 2004), and a thickness of 0.13 m. The base course was assumed to be 0.20 m thick and to have ν = 0.35. Modulus of the base layer was assumed to follow the non-linear elastic power function model described by Eqn. 2.2. For the base course, the parameter k_1 was assumed to be 27.8 MPa and k_2 was 0.5 (Huang 2004). The subgrade was assumed to be linearly elastic with a modulus of 48 MPa and ν = 0.45. The stress distribution predicted by MICH-PAVE is shown in Fig. 4.2, where vertical stress on the surface of the base layer and the subgrade layer is graphed as a function of the radial distance from the center of the applied load. Fig. 4.2 shows that the stress at the surface of the base course decreases from a maximum of 133 kPa with increasing distance from the load center. This maximum stress was applied in the LSME by applying a force of 6.7 kN with the loading plate.

4.1.2. Deflections

Vertical deflections of the pavement profile were measured on the base course surface directly beneath the loading plate and at distances of 200 and 300 mm from the centerline of the actuator. Vertical deflections of the subgrade surface were measured directly beneath the loading plate and at 200 mm from the centerline of the actuator. Linear variable differential transducers (LVDT) were used to measure deflections during each loading cycle. The LVDTs were capable of measuring deflections to 0.005 mm. Deflection measurements taken at the subgrade surface were accomplished by mounting small plates on each end of a thin rod running through a tube that extended through the overlying layer of base course. One plate rested on the subgrade surface while the LVDT rested on the other plate above the base course surface, with the tube eliminating friction between the base course and the rod and allowing the rod and plate assembly to move freely with the subgrade. The load and deflection data were collected

with a desktop personal computer running a LABVIEW 7.1 software program developed specifically for this application.

4.1.3. Data Inversion

Resilient modulus of the base layer was obtained by inversion with MICH-PAVE using the applied loads and the measured deflections. Accumulated plastic (non-recoverable) deflections were subtracted from the total deflections measured by the LSME to obtain the elastic deflections for analysis. The underlying sand layer was assumed to be linearly elastic and the modulus of the base course was assumed to follow the elastic power function in Eq. 2.2. The parameter k_2 was fixed at the value obtained from resilient modulus laboratory tests conducted per NCHRP 1-28A and the parameter k_1 was varied until the predicted deflections from MICH-PAVE were within 0.005 mm of the measured deflections in the LSME. This approach assumes k_2 varies within a narrow range for a particular material type (Huang 2004) and follows the approach described by Tanyu et al. (2003).

4.1.4. Placement of Base Course

Base course materials were placed in lifts approximately 0.10 m thick so that each material could be compacted uniformly. A vibratory plate compactor was used to achieve compaction and a nuclear density gage was employed to measure the dry unit weight and water content. Each lift was compacted at the optimum water content (w_o) until the dry unit weight was nearly 100% of the maximum dry unit weight ($\gamma_{d\ max}$) corresponding to standard Proctor effort. Soil specimens created for the NCHRP 1-28A resilient modulus tests were also compacted to $\gamma_{d\ max}$ and w_o allowing a more direct comparison of the M_R resulting from the two test methods.

For base course materials blended with cement or CKD, mixing the soil and additive was accomplished using a skid loader. The amount of material required for one lift was spread out on a concrete surface, and the appropriate amount of cement or CKD based on dry weight was blended with the base material having water content dry of optimum. Once the cement or CKD was blended thoroughly and the material had a uniform color, additional water was added to bring the water content of the mixture to optimum. Water was sprinkled evenly over the material while mixing continued with the skid loader. After mixing for approximately 20 minutes, the mixture was placed in the test pit and compacted immediately. The entire mixing and compacting procedure took about 45 min. Two separate 0.15 m thick lifts were mixed and placed in the test pit, with about 1 hour passing between compaction of subsequent lifts.

4.2. DURABILITY AND UNCONFINED COMPRESSIVE STRENGTH TESTS

Procedures outlined in the Soil-Cement Laboratory Handbook (PCA, 1992) for determining an optimum percentage of cement for construction applications were used to determine the optimum percentage of cement or CKD to use in the LSME tests. The PCA method involves conducting durability and UCS tests to determine an amount of cement to add. Trial percentages of cement or CKD to use in the durability and UCS tests were based on charts having inputs from the grain size distribution and the AASHTO classification of the soils. Specimens for both tests were prepared at optimum moisture content and maximum dry unit weight as determined by ASTM D 558: Standard Test Methods for Moisture-Density (Unit Weight) Relations of Soil-Cement Mixtures (Test Method B). The size of the cylindrical specimens created were 101.6 mm (4.0 in) in diameter and 114.3 mm (4.5 in) in length.

Durability tests consisted of creating cylinders of the stabilized base and subjecting them to either 12 cycles of wetting and drying or 12 cycles of freezing and thawing. The

cylinders were wire-brushed between cycles, and the percent mass loss was calculated. The wet-dry cycles were conducted according to ASTM D 559: Standard Test Methods for Wetting and Drying Compacted Soil-Cement Mixtures (Method B), and the freeze-thaw cycles were conducted according to ASTM D 560: Standard Test Methods for Freezing and Thawing Compacted Soil-Cement Mixtures (Method B). Durability test specimens were wrapped and moist cured for 7 days. For wet-dry cycles, specimens were submerged for 5 hours, and then oven-dried for approximately 42 hours. Wire brushing took place after the oven drying. For the freeze-thaw cycling, water-saturated felt pads were placed between specimens that were frozen for 24 hours, followed by thawing for 24 hours. Wire brushing took place after the thawing period.

The Short-Cut Test Procedures for Sandy Soils, described in Chapter 6 of the PCA Soil-Cement Laboratory Handbook, were used to determine a trial cement percentage of 5%. Therefore durability tests were carried out at two percentage points above and below 5%: i.e., 3% and 7%. The same percentages of cement were used for RPM. Since CKD was not expected to perform in the same way as cement, a larger range of percentages were tested based on typical amounts added in previous studies as described in Section 2. The percentages tested were 5%, 10% and 15% CKD added to both RPM and RSG.

UCS tests were performed as described by ASTM D 1633: Standard Test Methods for Compressive Strength of Molded Soil-Cement Cylinders (Method A). The same percentages of CKD and cement used for durability tests were also used for UCS tests. Specimens were submerged in water and soaked for approximately 4 hours, followed by capping with a sulfur compound. Specimens were sealed in plastic wrap and cured in a moist room for 7 and 28 days prior to testing.

4.3. CONVENTIONAL LABORATORY RESILIENT MODULUS TESTING

The base materials tested in the LSME were also tested by conventional laboratory methods according to the NCHRP 1-28A testing protocol (NCHRP 2004). The materials were tested under Procedure Ia, which applies to base and subbase materials. Cylindrical test specimens were molded with dimensions of 152 mm in diameter and 305 mm in height. All materials were compacted to 100% of maximum standard Proctor density at optimum water content. Both external and internal linear variable differential transducers were used for each specimen tested. The LVDTs had an accuracy of 0.005 mm. An MTS Systems Model 244.12 servo-hydraulic machine was used for loading the specimens. Loading sequences, confining pressure, and data acquisition were controlled by a PC equipped with Labview 8.5 software. The resilient moduli from the last five cycles of each test sequence were averaged to obtain the resilient modulus for each load sequence, and the data were fit to the power function described by Eqn. 2.2. A summary resilient modulus (SM_R) was also computed for each test corresponding to a bulk stress of 208 kPa, as suggested in Section 10.3.3.9 of NCHRP 1-28A. Further details on the laboratory testing methods are described by Camargo (2008) who performed the tests for unstabilized Class 5 gravel and RPM.

5. RESULTS AND ANALYSIS

5.1. DURABILITY AND UCS TESTS

The durability test results are presented in graphs showing the percent mass loss of the specimen increasing with the freeze-thaw or wet-dry cycle number. Results of freeze-thaw cycling are presented in Fig. 5.1a and b for RPM and RSG respectively, while similar graphs show the results of wet-dry cycling in Fig. 5.2a and b. The maximum amount of mass loss allowed by the PCA method is 14%, indicated by the dashed horizontal line.

For both RPM and RSG, specimens blended with cement were much more durable than specimens blended with CKD. All durability tests with cement resulted in less than 5% mass loss after 12 cycles, with the 3% cement specimen having the largest percent mass loss, and the 7% cement specimen having the lowest. There was no significant difference between the mass loss from wet-dry and freeze-thaw cycles for the RPM; however, RSG had approximately 2-3% higher mass loss from the freeze-thaw cycling.

The only durability tests involving CKD that resulted in mass loss less than 14% were the wet-dry tests with RPM. All other test specimens containing CKD disintegrated during wire brushing before completion of the test at 12 cycles. Increasing the CKD content improved durability of the RPM specimens, but this trend did not occur for RSG. For both wet-dry and freeze-thaw tests with RSG, 10% CKD resulted in the greatest number of cycles before disintegration occurred. The reason that RPM blended with CKD performed better during the wet-dry test than all other durability tests with CKD may be a result of the asphalt binder being heated in the drying oven, and binding the particles together. Freeze-thaw specimens were not placed in the oven.

The results of UCS tests with various amounts of CKD or cement are presented in Figs. 5.3a for RPM and 5.3b for RSG. UCS test results are presented for curing times of

7 and 28 days. Tests were also conducted on the control specimens from the cement durability tests, which were subjected to the wet-dry or freeze-thaw cycling, but did not undergo wire brushing, and had curing times of approximately 45 days.

RPM and RSG blended with cement had higher strengths than specimens blended with CKD. Strength increased with increasing cement content from 3% to 7% and also with increasing curing time. For specimens with cement, the RSG had lower 7 day curing strengths, but higher 28 day curing strengths than RPM. Very small amounts of strength gain took place in the RPM specimens blended with cement between 7 and 28 days. For both RSG and RPM, the durability test specimens (not brushed) showed the highest strength, demonstrating that strength was increasing even though the specimens were subjected to wet-dry and freeze-thaw cycles.

For RPM blended with CKD, strength increases with increasing CKD content for curing times of 7 and 28 days; however, no clear trend is seen with increasing CKD content for RSG. For both RPM and RSG, strength increases with increasing curing time perhaps due to delayed hydration caused by the sulfate content of CKD. Soaking had an adverse effect on the strengths of materials blended with CKD, demonstrated by comparing the strengths to samples that were not soaked and cured in a dry environment, similar to conditions tested in the LSME. These unsoaked strengths are shown for a CKD content of 10% blended with RSG at 7 and 28 days, and are more than twice the strength of the soaked samples.

The PCA Guide to Cement Treated Base (CTB) (Halsted et al. 2006) gives typical values of compressive strength for CTB between 2.1 and 5.5 MPa shown as dashed lines in Fig. 5.3, while the NCHRP Mechanistic-Empirical Pavement Design Guide (MEPDG) (ARA 2004) recommends a flexible pavement base course compressive strength of at least 5.2 MPa for chemically stabilized bases (Table 2.2.40). The only strengths obtained above 5.2 MPa were for RPM or RSG with cement having the higher

cement contents and/or the longer curing times. All tests conducted with cement were in or above the typical CTB range, but the only UCS tests with CKD above 2.1 MPa were the non-soaked LSME cured specimens for RSG, and RPM+15% CKD. UCS tests were also performed on the laboratory resilient modulus specimens having a height of 305 mm, a diameter of 152 mm and cured for 28 days. The UCS of these specimens was 1.42 MPa for RPM+10% CKD and 3.72 MPa for RSG+10% CKD.

The reason for the poor durability and lower strength of the specimens blended with CKD as compared to those blended with cement is likely due to expansion of the CKD. Table 5.5 contains the ratios of the final volume to the initial volume of the durability test control specimens that were not brushed. The final volume corresponds to the cycle indicated where the test ended based on reaching 12 cycles, or the brushed specimen falling apart and crumbling. The initial volume was measured after 7 days of curing, before beginning the wet-dry or freeze-thaw cycling. The ratios for specimens blended with CKD are greater than those blended with cement. The ratios for specimens blended with CKD are all above 1.0 indicating swelling, where specimens with cement contents swell slightly at lower cement contents, and shrink at higher cement contents. The CKD blended specimens of RSG swelled more than those of RPM.

Specimens of 100% CKD and a mix of 50% CKD and 50% uniform sand were created and cured for 28 days. These specimens had the same dimensions as the durability and UCS test specimens, and were cured in the same way (sealed with plastic, and placed in a curing room with 100% humidity). A significant increase in volume was observed for the specimens, shown in Fig. 5.4. Most of this expansion took place during the first 5 days of curing, and the amount of volume change appears to be related to the amount of CKD, because the 100% CKD samples experienced roughly twice the expansion of the samples with 50% CKD.

This increase in volume is probably due to the higher than average sulfur content of this particular CKD, reported as SO_3, which is 12.5% compared to an average of 6% (Table 3.3). Kota et al. (1996) observed that when sulfates are present in soil, pozzolanic reactions can be interrupted due to the formation of expansive minerals such as ettringite, which is a hexacalcium aluminate trisulfate hydrate, $(CaO)_6(Al_2O_3)(SO_3)_3 \cdot 32\ H_2O$, and is known to cause a volume increase in fresh, plastic concrete (PCA 2001). A large amount of water molecules are necessary for the formation of ettringite, and this may help to explain the lower strengths due to soaking as compared to the unsoaked "LSME" specimens shown in Fig. 5.3b. As per the ASTM standard, free water was made available to the specimens during the thawing cycle, so water was available for the formation of ettringite during both the freeze-thaw and the wet-dry durability tests.

The durability and UCS test results do not consistently show clear trends of increasing strength or durability with increasing CKD content unlike the same tests with cement, which do show a clear trend of greater strength and less mass loss with increasing cement content. This behavior may be a result of test specimens with higher CKD contents (i.e. 15%) swelling more than those with less CKD during curing and soaking.

Punthutaecha et al. (2006) determined volumetric swell expansion above 5% to be problematic, especially for low overburden structures such as pavements and embankments. Based on this criterion, the expansion measured with the CKD used in this study could very well cause distress to pavement structures.

The results of the durability and strength tests were used to select cement and CKD contents for use in the LSME. A cement content of 4% by weight was selected based on Fig. 39 of the PCA Soil-Cement Laboratory Handbook: *Indicated cement contents of soil-cement mixtures containing material retained on the No. 4 sieve*, where 4% was the minimum amount of cement indicated on this figure. Based on the durability and

strength testing, smaller percentages of cement would most likely provide acceptable results, and a minimum acceptable cement content for RPM and RSG could be the focus of additional research. A CKD content of 10% was selected for LSME testing, in an effort to avoid expansion with higher CKD contents, yet have enough free lime to bond the soil particles together. RSG+10% CKD was also shown to be more durable than 5% or 15% CKD during wet-dry testing.

5.2. LSME DEFLECTIONS

A graph showing total deflection and plastic deformation at the surfaces of the base and subgrade under the loading plate of the LSME as a function of the number of load cycles is displayed in Fig. 5.5 for a 0.30 m thick layer of Class 5 gravel. The total deflection is the maximum deflection measured during each 0.1 s loading cycle, and plastic deformation corresponds to the position of the layer surface measured during the 0.9 s rest period where only the plate seating load was applied. Plastic deformation of the base and subgrade accumulates monotonically during the test, with the highest rate of accumulation occurring in the first 50 cycles. The difference between the total deflection and plastic deformation is the elastic deflection. Elastic deflections graphed as a function of the number of load cycles is shown in Fig 5.6 for both 0.20 and 0.30 m thick layers of Class 5 gravel. Elastic deflections were directly measured at the surface of the base course and subgrade layer, and net base course elastic deflection was calculated as the difference between the surface and the subgrade deflections. Fig. 5.6 shows that surface elastic deflection, and therefore net base elastic deflection, decrease slightly throughout the course of the test due to the material becoming densely compacted under the loading plate, while the subgrade elastic deflection remains relatively constant. Elastic deflections for the 0.30 m thick layer are slightly less than the 0.20 m thick layer. This decrease in elastic deflection indicates a more extensive stress

distribution within the thicker base layer associated with the low strain in the bottom of the layer. A similar decrease was observed for unstabilized RPM and RSG.

10,000 cycles were applied to RPM and RSG blended with CKD and cement at curing times of 7, 14, 21 and 28 days for a total of 40,000 loading cycles on the same pavement profile. Fig. 5.7a and b compare total deflections and plastic deformations of RPM and RSG blended with CKD, and Fig. 5.8a and b compare the elastic deflections. Fig 5.7 shows an increase in the total accumulated plastic deformation over the duration of the four testing periods with RPM having plastic deformations nearly twice that of RSG blended with CKD. Fig. 5.8 shows a gradual decrease in the total and net base elastic deflections due to cementation of the soil and CKD, with the majority of the reduction in elastic deflection occurring before 14 days of curing. The subgrade elastic deflection remains nearly constant throughout the 28 day testing period.

A comparison of the elastic and plastic deflections at the base and subgrade surfaces between all materials tested in the LSME are shown in Fig. 5.9a and listed in Table 5.1, where the sum of the plastic and elastic deflection is equal to the total deflection. RSG has both the largest plastic and elastic deflections of the materials tested. The elastic deflections decrease with increasing layer thickness for Class 5 gravel, RPM, and RSG, but only the RSG has a smaller plastic deformation with increasing thickness. Stabilized materials were tested at one thickness of 0.30 m. Both plastic and elastic deflections of the stabilized materials were much lower than for the unstabilized materials due to the cementation characteristics of cement and CKD. Fig. 5.9b compares the deflections of the stabilized materials at the initial 7 day and final 28 day curing times. The elastic deflections of the base course materials are less at 28 days than at 7 days except for RPM and cement, where the elastic deflections remained the same. Greater plastic deflection for both the base and the subgrade is seen at 7 days than at 28 days due to the effect of the initial loading cycles increasing the density

and settling of the loading plate as well as increased curing time. The elastic deflection of the subgrade was nearly consistent between tests for stabilized materials.

5.3. RESILIENT MODULUS COMPARISON FROM LSME AND LABORATORY TESTING

The relationship between the resilient modulus and bulk stress as described by Eqn. 2.2 is shown in Figs. 5.10a, b and c for Class 5 gravel, RPM and RSG respectively resulting from both the LSME and laboratory (NCHRP 1-28A) tests. The LSME relationships calculated by MICH-PAVE based on measured loads and deflections are shown for unstabilized base materials having thicknesses of 0.20 and 0.30 m, along with 10% CKD stabilized materials at 0.30 m thick and cured for 28 days. Also included are the relationships obtained directly from laboratory resilient modulus tests conducted by Camargo (2008) for the unstabilized base materials using internal LVDTs. Table 5.2 lists the parameters k_1 and k_2 used in Eqn. 2.2, where the k_2 from the laboratory test was used for the LSME backcalculation.

For unstabilized materials without cement or CKD, the elastic modulus increases with the bulk stress; however, the elastic modulus is not sensitive to bulk stress for stabilized materials, as shown by the relationship being a horizontal line for base materials blended with 10% CKD. The LSME resilient modulus of each base material is significantly higher when 10% CKD is added, even at higher bulk stresses. For unstabilized base materials, the elastic modulus measured in the LSME is sensitive to the thickness of the base layer, where thicker layers have a higher modulus at a given bulk stress. This sensitivity can be explained by the differing level of strain between layers of varying thickness under the same applied load, which is known to affect the elastic modulus of granular materials (Seed and Idriss 1970; Hardin and Drnevich 1972; Tanyu et al. 2003). Under the same applied surface load, a lower vertical strain will exist

in thicker layers due to greater stress distribution in a thicker layer compared to a thinner layer.

Because of the variation of resilient modulus with bulk stress, a summary resilient modulus (SM_R) of each test was computed as suggested in Section 10.3.3.9 of NCHRP 1-28A, where for base materials the SM_R corresponds to a bulk stress of 208 kPa. The SM_R resulting from LSME and laboratory tests are compared in Fig 5.11a and b, and also are listed in Table 5.2. Fig. 5.11a compares the SM_R of unstabilized LSME and laboratory tests conducted with both externally and internally mounted LVDTs, along with the stabilized LSME test results. Stabilized laboratory tests using external and internal LVDTs are compared with stabilized LSME tests in Fig. 5.11b. During laboratory testing, external LVDTS were mounted on the plunger outside the chamber and rested on the cover plate measuring deformations of the entire specimen length, where internal LVDTs were placed at quarter points of the specimen to determine deformations over half the specimen length.

For tests conducted without cement or CKD, the resilient modulus of 0.30 m thick layers is higher than the laboratory test results, but no clear trend is seen between the laboratory tests and the 0.20 m thick layer tests. The laboratory SM_R is closer to the LSME SM_R resulting from the 0.20 m thickness for unstabilized Class 5 gravel and RPM, but closer to the 0.30 m thick result for RSG. Both the internal laboratory and LSME results show RSG having the lowest SM_R, and RPM having the highest with Class 5 gravel in between. The SM_R increases significantly when cement or CKD is added to the base materials. RSG+10% CKD demonstrated the greatest increase in LSME SM_R over the unstabilized 0.30 m layer with the ratio of stabilized SM_R to unstabilized SM_R being 6.1. The lowest ratio of stabilized LSME SM_R to unstabilized LSME SM_R equal to 4.6 was for RSG+4% cement.

The internal SM_R of stabilized laboratory tests are much greater than the SM_R obtained from the stabilized LSME tests, as shown in Fig. 5.11b. The greatest difference is for RSG+10% CKD where the SM_R from the laboratory test is 37,790 MPa compared to the LSME SM_R of 1340 MPa. RPM+10% CKD demonstrated the least difference, with a laboratory SM_R of 5530 MPa compared to the LSME SM_R of 1080 MPa.

The SM_R of the laboratory tests based on internal and external LVDTs are reported in Table 5.3, along with the ratios of internal SM_R to external SM_R. For all stabilized tests, the external SM_R is less than that determined with the LSME and the internal LVDTs. The ratios of internal SM_R to external SM_R ranged from 12.3 to 58.1, indicating a very large difference between the two measurements. Camargo (2008) compared the SM_R from internal and external LVDTs for RPM and RSG blended with fly ash, and reported ratios of internal to external SM_R ranging from 4.0 to 18.3. Differences between the two measurements were attributed to the external LVDTs being affected by bedding errors, sample end effects and machine compliance. Some of these same factors could have affected the LSME SM_R, where the LVDTs were placed on top of the steel plate applying the load to the base surface. The external SM_R is much closer to the LSME SM_R than the internal SM_R.

The difference in curing conditions and the sensitivity to moisture of the specimens blended with CKD may also have been a factor between the laboratory and LSME test results. Laboratory samples were sealed in plastic and placed in a 100% humidity curing room, where the LSME was covered with a moist fabric. The water content of the stabilized LSME samples decreased 2 to 3 % between mixing and removing after 28 days of curing. The more controlled curing conditions and the plastic holding in the moisture of the laboratory specimens could have resulted in more efficient hydration processes.

A third factor that may cause a higher stabilized SM_R from laboratory tests is explained by more thorough mixing of the laboratory specimens as compared to the LSME specimens. The laboratory specimens were mixed with cement or CKD at a lower initial water content, allowing a more thorough blending of the soil and fine powder material. The larger LSME specimens were mixed at a higher water content due to the material being stored outside. This extra moisture likely caused the cement or CKD to flocculate and clump together, not mixing as well throughout the material. Mixing with the skid loader was also not as efficient as hand tools used for the smaller laboratory specimens. The LSME is considered to be a more realistic simulation of field conditions with respect to mixing and curing, and several studies have indicated stiffness to be less for field mixed samples than for laboratory mixed samples. Li et al. (2007) reported a M_R of field mixed specimens 25% lower than that of laboratory mixed specimens.

Both LSME and laboratory tests show the same pattern for stabilized materials, where 10% CKD results in a greater stiffness than with 4% cement for RSG, while the opposite effect is seen for RPM. RPM+4% cement had a greater LSME SM_R at 28 days (1220 MPa) than RPM+10% CKD (1080 MPa), while RSG+4% cement had a smaller SM_R (1010 MPa) than RSG+10% CKD (1340 MPa). One reason for this behavior may be that the greater volume of CKD than cement contributes to stiffness when blended with RSG due to pores being filled.

LSME tests with cement and CKD were conducted at 7, 14, 21 and 28 days to evaluate the effects of curing on stiffness. An increase in the SM_R between 7 and 28 days is observed for each stabilized base course material except for RPM+4% cement, demonstrated in Fig 5.12. RPM and RSG blended with CKD show a greater increase in stiffness than when blended with cement, with RSG+10% CKD having the greatest rate of increase. RPM and RSG blended with cement obtain higher early (7 day) stiffness than with CKD, after which a modest increase was seen for RSG and a slight decrease

in stiffness observed for RPM. The decreases in stiffness seen between two of the cement blended tests may be due to bonds being broken by the repeated action of the loading plate.

Fig. 5.13 demonstrates the effect of soaking stabilized materials in the LSME test pit after 28 days of curing. Water was applied to the stabilized layers of RPM and RSG until the layer was saturated, shortly after which cyclic loading was applied to determine the resilient modulus. This “soaked” test was conducted for RPM stabilized with cement and CKD and for RSG stabilized with CKD. A decrease in the resilient modulus was observed for all three saturated tests, followed by an increase after 7 days of drying. RSG+10% CKD experienced the greatest decrease upon soaking (a 36% drop from the 28 day stiffness), while RPM+4% cement experienced the smallest decrease (a 24% drop from the 28 day stiffness). RPM+10% CKD experienced a 27% decrease from the 28 day stiffness. All three stabilized materials increased in stiffness as compared to soaked stiffness after 7 days of drying, as demonstrated in Fig. 5.13. The tests with CKD recovered more of the 28 days stiffness than the test with RPM and cement, although the one soaked test with cement experienced the smallest percent decrease from 28 day stiffness. This variation in stiffness with wetting and drying is expected to simulate a field situation where the base course layer becomes saturated for a short period during heavy rains or melting snow, followed by a period of draining and drying.

The NCHRP MEPDG gives typical resilient modulus values for unbound granular soils according to the AASHTO soil classification. For an A-1-a soil such as Class 5 gravel or RPM, a typical resilient modulus is 280 MPa and for A-2-4 such as RSG a typical resilient modulus is 220 MPa. The summary resilient modulus measured in the LSME is also 220 MPa for the 0.30 m thickness of RSG, and the 0.20 m thicknesses of RPM and Class 5 gravel are 310 MPa and 280 MPa respectively. Therefore, the

resilient modulus of unbound granular materials are determined to be very close to expected values as determined by the LSME for typical base course thicknesses.

For soil-cement a typical resilient modulus is 3450 MPa and 6900 MPa for cement stabilized aggregate. The PCA Guide to CTB also gives a typical modulus range of 4100 to 6900 MPa. The summary resilient moduli of stabilized materials measured in the LSME were well below these numbers, ranging from 1010 MPa to 1340 MPa. However, laboratory results for the same materials were within or above the typical ranges given, with the lowest laboratory resilient modulus for RPM+10% CKD being 5530 MPa. Therefore, caution should be exercised when designing pavements with stabilized bases using the resilient modulus determined from common laboratory test methods, especially with internal LVDTs, because the laboratory modulus may be significantly higher than in an actual pavement structure.

5.4. DETERMINATION OF RECYCLED BASE COURSE LAYER COEFFICIENTS

Determining the appropriate thickness of the pavement layers based on engineering properties is a critical task in the design of pavement structures. Methods for design of flexible pavement structures may vary among states, but a commonly used design guideline in the United States, especially for city and county roads, is the AASHTO Guide for Design of Pavement Structures. In the AASHTO design procedure, the structural capacity of a specific material layer is described by the structural number of that layer (SN_i) calculated by multiplying the layer thickness (D_i) with structural layer coefficient (a_i). The layer coefficient depends on the mechanical properties of the materials comprising the pavement layer (AASHTO, 1993). The total SN for the entire pavement structure is the summation of the structural number of each pavement layer:

$$SN = SN_1+SN_2m_2+SN_3m_3 = a_1 D_1 + a_2 D_2 m_2 + a_3 D_3 m_3 \quad (5.1)$$

where m_i is the drainage modification factor, a_i is the layer coefficient, and D_i is the thickness of layer i. For the base materials used in this study, the drainage modification factors were assumed to be 1. In Eqn. 5.1, the subscript 1 corresponds to the asphalt surface layer, 2 for the base layer and 3 for the subbase if included. The subgrade is not considered in Eqn. 5.1. Design thicknesses are determined by inputting thicknesses into equation 5.1 to calculate SN, and then ensuring that the calculated SN is greater than or equal to the required SN. Typically the required SN of a pavement system is determined based on estimated traffic, serviceability loss, and the effective roadbed resilient modulus (AASHTO 1993).

The layer coefficient has been shown to be a function of resilient modulus of a granular base layer (Rada and Witczak 1981) according to the following relationship:

$$a_2 = 0.249 \log M_R - 0.977 \quad (5.2)$$

where M_R is the resilient modulus (in units of psi) of the base material. The structural layer coefficients to be used in the AASHTO method were calculated using Eqn. 5.2 using the M_R from Fig. 5.14, which shows the relationship between the resilient modulus and base layer thickness. For the stabilized base course materials, the resilient modulus does not vary with thickness, as shown previously in Fig. 5.10, and this relationship is again seen as a horizontal line in Fig. 5.14. However, the resilient modulus of the unbound granular materials do vary with thickness, because under the same applied surface load a lower vertical strain will exist in thicker layers due to greater stress distribution as compared to a thinner layer. Fig. 5.14 shows the summary resilient modulus increasing with base layer thickness for Class 5 gravel, RPM and RSG. The SM_R for layer thicknesses of 0.20 m and 0.30 m were determined from the LSME, while base course thicknesses other than 0.20 m and 0.30 m were predicted using a backbone curve and numerical analysis with MICH-PAVE described in Appendix A.

Since the M_R of the unstabilized granular materials varies with thickness, the layer coefficient also varies with thickness as shown in Fig. 5.15. Since the layer coefficient is used to determine the layer thickness in a pavement structure, a trial and error procedure can be performed during pavement design to ensure the design layer thickness is calculated with a layer coefficient that corresponds to a thickness that is greater than or equal to the thickness given in Fig. 5.15.

The SN of the recycled base layer was calculated for each material tested in the LSME by multiplying the layer coefficient obtained from Eqn. 5.2 by the layer thickness (using English units of inches), shown in Table 5.4. This table, along with Fig. 5.15, show that RSG has the lowest structural numbers and layer coefficients of materials tested, and using a layer of unstabilized RSG less than 0.20 m thick is not recommended. However, RSG blended with 10% CKD becomes the stiffest material tested, having the greatest layer coefficients. Class 5 gravel and unstabilized RPM have relatively similar layer coefficients which increase with increasing layer thickness in a similar manner. All stabilized materials with either cement or CKD have greater layer coefficients than the unstabilized materials, ranging from 0.31 for RSG+4% cement to 0.34 for RSG+10% CKD. As the unstabilized materials increase in thickness, their layer coefficients approach that of the stabilized layer coefficients. Therefore stabilizing thinner layers of base course materials will result in a greater increase in stiffness than for thicker layers.

Due to lack of field experience and unknown long-term performance of the stabilized base course materials, caution and engineering judgment should be exercised when using the layer coefficients of stabilized materials given in Table 5.4, possibly reducing the layer coefficient by a factor of safety.

6. SUMMARY AND CONCLUSIONS.

This investigation dealt with the determination of the resilient modulus of two recycled roadway materials with and without the addition of cement and cement kiln dust (CKD): recycled pavement material (RPM) and recycled road surface gravel (RSG). The main objective was to determine a field-operative resilient modulus for use in pavement design methods for both the unbound and stabilized recycled materials tested. To meet this objective, the modulus of recycled materials with and without cement and CKD was determined from a Large Scale Model Experiment (LSME) and compared with the resilient modulus obtained from the laboratory test method described by NCHRP 1-28A. Results of wet-dry and freeze-thaw durability tests were used in selecting a portland cement content of 4% by weight and a CKD content of 10% by weight to be used in the stabilization of RPM and RSG. The stiffness at curing times of 7 and 28 days was evaluated, and the summary resilient modulus corresponding to a bulk stress of 208 kPa was used to calculate AASHTO layer coefficients for use in pavement layer thickness design. Class 5 gravel (similar to AASHTO Grading C), with a conventional base material gradation employed in Minnesota, was used as a reference material.

The following behavioral trends were observed for the materials tested in this program:

1. Durability tests indicated that RPM and RSG blended with cement were more durable than when blended with CKD based on the percent mass loss. Freeze-thaw testing resulted in greater mass loss than the wet-dry testing. Significant increases in test specimen volumes were observed, where increasing CKD content resulted in greater volume increases. This volume change is most likely the result of the formation of expansive minerals such as ettringite due to the higher than average sulfur content of the CKD used in this study. Caution should

be used when stabilizing a base course with an expansive material such as CKD with higher sulfur contents, which may result in damage to the pavement structure. Further research should be conducted on field pavement test sections focusing on cracking or heaving of the CKD stabilized soil and with CKDs of lower sulfur content. Results of durability and strength testing were used to select percentages of 4% cement and 10% CKD for use in the large scale testing.

2. Both RPM and RSG had plastic deformations greater than Class 5 base, where plastic deformation for RPM was approximately 46% greater than for Class 5 base, and RSG had plastic deformations approximately 189% greater. The greatest plastic deformation measured in the LSME was for RSG. The plastic deformation of both the base and subgrade decrease significantly with the addition of cement or CKD to the base, where RSG with CKD had the least plastic deformation overall.
3. RSG had the largest elastic deformations, resulting in the lowest modulus (120 MPa for 0.20 m thickness and 220 MPa for 0.30 m thickness) and RSG blended with CKD at 28 days of curing had the highest resilient modulus (1340 MPa). RPM had a modulus slightly greater than Class 5 base for each thickness. For all three materials tested without cement or CKD, the modulus increased with an increase in base layer thickness. The modulus of RPM and RSG increased significantly with the addition of cement and CKD, and continued to increase in stiffness over a curing time of 28 days, with the exception of RPM blended with cement. For 0.30 m thick layers, the modulus of RPM with 4% cement after 28 days of curing was 2.4 times higher than unstabilized RPM, while RPM with 10% CKD was 2.1 times greater. The modulus of RSG with cement increased by a factor of 4.6 compared to unstabilized RSG, and by a factor of 6.1 for RSG with

CKD. RPM and RSG blended with CKD gained greater stiffness compared to cement, although the cement resulted in a higher 7 day modulus.

4. The summary moduli determined from the LSME tests with stabilized materials were significantly less than the summary moduli measured in the laboratory resilient modulus tests measured with internal LVDTs. The LSME SM_R was larger than, but much closer to, the laboratory external SM_R. Other factors that may contribute to the difference between the laboratory and LSME tests are mixing of the RPM and RSG with cement and CKD and the curing conditions. The LSME modulus is expected to be closer to actual field conditions than the laboratory test, and therefore caution is recommended when using laboratory resilient modulus values for design, specifically those determined with internal LVDTs.
5. The resilient modulus was found to increase with the bulk stress for all three granular base course materials (i.e., without cement or CKD) indicating the nonlinearity or stress-dependency of these materials. However, with the addition of cement or CKD, the resilient modulus did not show stress dependency for a range of stresses typically resulting from wheel loads and was considered to be a linear elastic material as confirmed by laboratory resilient modulus tests and varying stress applied to the LSME specimen.
6. AASHTO layer coefficients were calculated from the resilient modulus determined in the LSME for use in pavement thickness design. The layer coefficients for the unstabilized materials increased with layer thickness, reflecting the increase in modulus with a thicker layer. Layer coefficients for RPM and RSG blended with cement and CKD remain constant with layer thickness, and are greater than unstabilized layer coefficients, indicating increased structural capabilities.

This study has shown that the addition of cement and/or CKD can significantly improve the engineering properties of different types of soils, and has the potential to allow the greater use of recycled materials such as RSG and RPM in the reconstruction of roads, minimizing construction costs and environmental impacts. However, the low durability and expansion of recycled materials blended with CKD should be investigated further, because swelling of soils can cause damage to pavement structures.

REFERENCES

AASHTO (1993). *Guide for Design of Pavement Structures*, American Association of State Highway and Transportation Officials, Washington, D.C.

AASHTO (2001). *Standard Specifications for Transportation Materials and Methods of Sampling and Testing, 21st Ed.*, American Association of State Highway and Transportation Officials, Washington, D.C., *Part 1, Specifications*, M 147-65

Adaska, W.S., Taubert, D.H. (2008). "Beneficial Uses of Cement Kiln Dust," *Cement Industry Technical Conference Record*, May 2008, pp 210-228.

Analog Devices (2007). Analog Devices, Inc. Web Site, http://www.analog.com.

ARA (2004). "Guide for Mechanistic-Empirical Design of New and Rehabilitated Pavement Structures," NCHRP Project 1-37A, prepared for National Cooperative Highway Research Program, Washington D.C.

Baghdadi, Z.A., Fatani, M.N., and Sabban, N.A. (1995). "Soil Modification by Cement Kiln Dust," *Journal of Materials in Civil Engineering*, ASCE, pp. 218-222.

Baugh, J. (2008). "Suitability of Cement Kiln Dust for Reconstruction of Bituminous Roads," *MS Thesis*, University of Wisconsin-Madison, Madison, WI.

Bhatty, J.I., Bhattacharja, S., and Todres, H.A. (1996). *Use of Cement Kiln Dust in Stabilizing Clays*, RP343, Portland Cement Association, Skokie, IL.

Camargo, F. (2008). "Strength and Stiffness of Recycled Base Materials Blended with Fly Ash," *MS Thesis*, University of Wisconsin-Madison, Madison, WI.

Cooley, D. (2005). "Effects of Reclaimed Asphalt Pavement on Mechanical Properties of Base Materials," *MS Thesis*, Brigham Young University, Provo, UT.

Edil, T. B. and Luh, G. F. (1978). "Dynamic Modulus and Damping Relationships for Sands," Proceedings of the Specialty Conference on Earthquake Engineering and Soil Dynamics, ASCE, Reston, VA, pp. 394-409.

Epps, J. A. (1990). "Cold-Recycled Bituminous Concrete Using Bituminous Materials," *NCHRP Synthesis of Highway Practice 160*, National Cooperative Highway Research Program, Washington, D.C.

Finn, F. N., Saraf, C. L., Kulkarni, R., Nari, K., Smith, W., and Abdullah, A. (1986). "Development of Pavement Structural Subsystems," *NCHRP Report 291*, Transportation Research Board, Washington, D.C.

Guthrie, S., Brown, A., and Eggett, D. (2007). "Cement Stabilization of Aggregate Base Material Blended with Reclaimed Asphalt Pavement," *Journal of the Transportation Research Board*, 2026, pp. 47-53.

Halsted, G., Luhr, D., Adaska, W. (2006). *Guide to Cement-Treated Base (CTB)*, Publication EB236, Portland Cement Association, Skokie, IL.

Hardin, B. O. and Drnevich, V. P. (1972). "Shear Modulus and Damping in Soils: Design Equations and Curves," *Journal of Soil Mechanics and Foundations Division*, ASCE, Vol. 98, No. 7, pp. 667-692.

Harichandran, R. S., G. Y. Baladi, and M. Yeh, (1989). "Development of a Computer Program for Design of Pavement Systems Consisting of Bound and Unbound Materials," Department of Civil and Environmental Engineering, Michigan State University, Lansing, Michigan.

Hatipoglu, B., Edil, T., and Benson, C. (2008). "Evaluation of Base Prepared from Road Surface Gravel Stabilized with Fly Ash," *GeoCongress 2008 ASCE Geotechnical Special Publication,* 177, New Orleans, LA, pp. 288-295.

Haynes, J. G., Yoder, E. J. (1963). "Effects of Repeated Loading on Gravel and Crushed Stone Base Course Materials Used in the AASHO Road Test." *Hwy. Res. Rec. 39*.

Haynes, B. W., and Kramer, G. W. (1982). "Characterization of U. S. Cement Kiln Dust," *Information Circular #8885*, Bureau of Mines, U. S. Department of Interior, Washington, DC.

Hicks, R. G. (1970). "Factors Influencing the Resilient Properties of Granular Materials," *PhD Thesis*, University of California, Berkeley, Berkeley, CA.

Hicks, R. G., Monismith, C. L. (1971). "Factors Influencing the Resilient Properties of Granular Materials," *Hwy. Res. Rec. 345*, pp 15-31.

Huang, Y. (2004). *Pavement Analysis and Design*, 2nd Ed., Prentice-Hall, Inc., Upper Saddle River, New Jersey.

Kamal, M. A., Dawson, A. R., Farouki, O.T., Hughes, D.A.B., and Sha'at, A. A. (1993). "Field and Laboratory Evaluation of the Mechanical Behavior of Unbound Granular Materials in Pavements," *Transportations Research Record 1406*, Transportation Research Board, Washington, D.C., pp 88-97.

Kearney, E.J. and Huffman, J.E. (1999). "Full-Depth Reclamation Process," *Journal of the Transportation Research Board,* 1684*,* pp.203-209.

Kim, D. S., and Stokoe II, K. H. (1992). "Characterization of Resilient Modulus of Compacted Subgrade Soils Using Resonant Column and Torsional Shear Tests," *Transportation Research Record 1369*, Transportation Research Board, National Research Council, Washington, DC, pp. 83-91.

Kim, W., Labuz, J., and Dai, S. (2007). "Resilient Modulus of Base Course Containing Recycled Asphalt Pavement," *Journal of the Transportation Research Board,* 2005, pp. 27-35.

Kokusho, T. (1980). "Cyclic Triaxial Test of Dynamic Soil Properties for Wide Strain Range," *Soils and Foundations*, Vol. 20, No. 2, pp. 45-60.

Kolisoja, P. (1997). “Resilient Deformation Characteristics of Granular Materials,” *PhD thesis*, Tampere University of Technology, Pub. No. 223, Tampere, Finland.

Kota, Prakash, B.V.S., Hazlett, Darren, and Perrin, Les (1996). “Sulfate-Bearing Soils: Problems with Calcium-Based Stabilizers,” *Transportation Research Record 1546*, 1996, pp 62-69.

Li, L., Benson, C. H., Edil, T. B., Hatipoglu, B. (2008). ‘‘Sustainable Construction Case History: Fly Ash Stabilization of Recycled Asphalt Pavement Material,’’ *Geotechnical and Geological Engineering*, Vol. 26, No. 2, pp. 177-188.

Luhr, D. (2004). “Recycling Roads Saves Money and Natural Resources,” *Public Works*, Vol. 136, No. 5, pp. 115-117.

Mallick, R.B., Teto, M.R., Kandhal, P.S., Brown, E.R., Bradbury, R.L. and Kearney, E.F. (2002). “Laboratory Study of Full-Depth Reclamation Mixes,” *Journal of the Transportation Research Board,* 1813*,* pp.103-110.

Mitchell, J. (1993). *Fundamentals of Soil Behavior*, 2nd ed., John Wiley and Sons, Inc. New York, New York.

Moosazedh, J., and Witczak, M. (1981). “Prediction of Subgrade Moduli for Soil That Exhibits Nonlinear Behavior”, *Transportation Research Record 810*, 1981, pp. 10-17.

MnDOT (2005). *Standard Specifications for Construction*, Minnesota Department of Transportation, St. Paul, MN.

Muhanna, A., Rahman, M., and Lambe, P. (1998). “Model for Resilient Modulus and Permanent Strain of Subgrade Soils,” *Transportation Research Record 1619*, 1998, pp. 85-93.

NCHRP (2004). “Laboratory Determination of Resilient Modulus for Flexible Pavement Design,” *National Cooperative Highway Research Program Research Results Digest*, 285, pp 1-48.

Portland Cement Association, (2001). *Ettringite Formation and the Performance of Concrete,* IS417.

Portland Cement Association, (1992). *Soil-Cement Laboratory Handbook*.

Punthutaecha, K., Puppala, A.J., Vanapalli, S.K., and Inyang, H. (2006). “Volume Change Behaviors of Expansive Soils Stabilized with Recycled Ashes and Ffibers,” *Journal of Materials in Civil Engineering*, Vol. 18, No. 2, pp. 295-306.

Rada, G. and M. W. Witczak, (1981). “A Compressive Evaluation of Laboratory Resilient Moduli Results for Granular Materials,” *Transportation Research Record No. 810*, Transportation Research Board, Washington D.C.

Richart, F. E. Jr., Hall, J. R., and Woods, R. D. (1970). *Vibrations of Soils and Foundations,* Prentice Hall, Inc., Eaglewood Cliffs, NJ.

Santamarina, J.C., Klein, K.A., and Fam, M.A. (2001). *Soils and Waves*, John Wiley & Sons Ltd., West Sussex, England, pp 488.

Sawangsuriya, A., and Edil, T. B. (2005). "Evaluating Stiffness and Strength of Pavement Materials," *Geotechnical Engineering*, 158(4), 217-230.

Sawangsuriya, A., Edil, T. B., Bosscher, P. J. (2005). "Relationship between Soil Stiffness Gauge Modulus and Other Test Moduli for Granular Soils," *Transportation Research Record* 1849, Transportation Research Board, National Research Council, Washington, DC, pp. 3-10.

Schuettpelz, C. (2008). "Evaluation of the Influence of Geogrid Reinforcement on Stiffness in Compacted Base Course Material," *MS Thesis*, University of Wisconsin-Madison, Madison, WI.

Seed, H. B., Mitry, F. G., Monismith, C. L., and Chan, C. K. (1965). "Predictions of Pavement Deflection From Laboratory Repeated Load Tests," *Rep. No. TE-65-6*, Soil Mech. and Bituminous Mat. Res. Lab, University of California, Berkeley, Berkeley, CA.

Seed, H. B. and Idriss, I.M. (1970). "Soil Moduli and Damping Factors for Dynamic Response Analyses," *Report No. EERC 70-10*, University of California, Earthquake Engineering Research Center, Berkeley, CA.

Sreekrishnavilasam, A., King, S., and Santagata, M. (2006). "Characterization of Fresh and Landfilled Cement Kiln Dust for Reuse in Construction Applications," *Engineering Geology*, vol. 85, pp. 165-173.

Taha, R., Ali, G., Basma, A., and Al-Turk, O. (1999). "Evaluation of Reclaimed Asphalt Pavement Aggregate in Road Bases and Subbases, *Journal of the Transportation Research Board,* 1652, pp. 264-269.

Taha, R. (2003). "Evaluation of Cement Kiln Dust-Stabilized Reclaimed Asphalt Pavement Aggregate Systems in Road Bases," *Transportation Research Record*, Journal of the Transportation Research Board, TRB Record 1819, Washington D.C., pp. 11-17.

Tanyu, B.F. (2003). "Working Platforms for Flexible Pavements Using Industrial By-Products," *PhD. Thesis*, University of Wisconsin-Madison, Madison, WI.

Tanyu, B. F., Kim, W. H., Edil, T. B., and Benson, C. H. (2003). "Comparison of Laboratory Resilient Modulus with Back-Calculated Elastic Moduli from Large-Scale Model Experiments and FWD Tests on Granular Materials," Resilient Modulus Testing for Pavement Components, *ASTM STP 1437, Paper ID 10911*, G. N. Durham, A. W. Marr, and W. L. De Groff, Eds., ASTM International, West Conshohocken, PA.

Tanyu, B.F., Benson, C.H., Edil, T.B., and Kim, W. (2004). "Equivalency of Crushed Rock and Three Industrial By-Products Used for Working Platforms During Pavement Construction," *Transportation Research Record 1874*, pp 59-69.

Thom, N. H. (1988). "Design of Road Foundations," *PhD Thesis*, Dept. of Civil Engineering, University of Nottingham, Nottingham, England.

Thom, N. H. and Brown, S. F. (1987). "Effect of Moisture on the Structural Performance of a Crushed-Limestone Road Base," *Transportation Research Record 1987*, Transportation Research Board, Washington, D.C., pp 50-56.

Todres, H. A., Mishulovich, A., and Ahmad, J. (1992). *Cement Kiln Dust Management: Permeability*, Research and Development Bulletin RD103T, Portland Cement Association, Skokie, IL.

Wen, H. and Edil, T.B. (2009). "Sustainable Reconstruction of Highways with In-Situ Reclamation of Materials Stabilized for Heavier Loads," *BCR^{2}A'09, Proceedings of the 8th International Conference on the Bearing Capacity of Roads, Railways, and Airfields*, Champaign, IL

Wen, H., Tharaniyil, M., Ramme, B. and Krebs, U. (2004). "Field Performance Evaluation of Class C Fly Ash in Full-Depth Reclamation: Case History Study," *Journal of the Transportation Research Board,* 1869, pp. 41-46.

Zaman, M.Z., Zhu, J., and Laguros, J.G. (1999). "Durability Effects on Resilient Moduli of Stabilized Aggregate Base," *Transportation Research Record*, Journal of the Transportation Research Board, TRB Record 1687, Washington D.C., pp. 29-38.

TABLES

Table 3.1. Index properties for Class 5 base, RPM, and RSG.

Sample	D_{50} (mm)	C_u	C_c	G_s	w_{opt} (%)	$\gamma_{d\ max}$ (kN/m^3)	Asphalt Content (%)	LL (%)	PL (%)	Gravel Content (%)	Sand Content (%)	Fines Content (%)	USCS Symbol	AASHTO Symbol
Class 5 base	2.25	33.3	0.7	2.72	5.0	20.9	-	NP	NP	36.6	59.3	4.1	SP	A-1-a
RPM	3.89	89.5	2.5	2.64	7.5	21.2	4.6	NP	NP	46.0	43.0	10.6	GW-GM	A-1-a
RSG	0.80	40.0	1.0	2.73	7.5	22.6	-	21	14	28.6	59.0	12.4	SC-SM	A-2-4

D_{50} = median particle size, C_u = coefficient of uniformity, C_c = coefficient of curvature, G_s = specific gravity, w_{opt} = optimum water content, $\gamma_{d\ max}$ = maximum dry density, LL = liquid limit, PL = plastic limit, NP = nonplastic.

Note: Particle size analysis conducted following ASTM D 422, G_s determined by ASTM D 854, $\gamma_{d\ max}$ and w_{opt} determined by ASTM D 698, USCS classification determined by ASTM D 2487, AASHTO classification determined by ASTM D 3282, asphalt content determined by ASTM D 6307, and Atterberg limits determined by ASTM D 4318.

Table 3.2. Maximum dry unit weights, optimum water contents and optimum CBRs of recycled base materials.

Material	Optimum Water Content* (%)	Maximum Dry Unit Weight (kN/m^3)	CBR (%)
Class 5 base	5.0	20.9	10
RPM	7.5	21.2	22
RPM + 10% CKD	7.7	20.9	NT**
RPM + 4% Cement	7.5	20.8	
RSG	7.5	22.6	
RSG + 10% CKD	9.5	20.9	
RSG + 4% Cement	8.4	21.2	

* Optimum water content for dry unit weights.
** NT = not tested

Table 3.3. CKD physical properties and chemical compositions.

Component or Property (% by weight)	Alpena CKD	Typical CKD	CKD used by Baugh (2008)
$CaCO_3$	54.1	44.0	54.4
SiO_2	12.0	13.6	14.7
Al_2O_3	4.4	4.5	3.7
Fe_2O_3	2.1	2.1	2.2
MgO	1.7	1.3	2.3
SO_3	12.5	6.0	10.5
Free CaO	13.9	8.1	-
LOI[1]	10.7	21.6	9.41
Total alkali[2]	2.33	3.32	3.57

Alpena CKD data provided by manufacturer.

Typical CKD data reproduced from Sreekrishnavilasam et al. (2006) and Haynes and Kramer (1982).

[1]LOI = loss on ignition;
[2]Total alkali = $Na_2O + 0.658 \times K_2O$;

Table 5.1. Measured Deflections after 10,000 LSME Loading Cycles.

Base Material	Layer Thickness (m)	Base Elastic (mm)	Base Plastic (mm)	Subgrade Elastic (mm)	Subgrade Plastic (mm)	Total Deflection (mm)
Class 5 Gravel	0.20	0.065	0.630	0.155	0.215	1.065
	0.30	0.060	0.760	0.150	0.130	1.100
RPM	0.20	0.050	0.965	0.155	0.170	1.345
	0.30	0.075	1.060	0.140	0.070	1.310
RSG	0.20	0.165	1.980	0.160	0.215	2.520
	0.30	0.120	1.655	0.140	0.120	2.035
RPM + CKD	0.30	0.030	0.075	0.065	0.095	0.265
RSG + CKD	0.30	0.025	0.035	0.045	0.020	0.125
RPM + Cement	0.30	0.020	0.165	0.040	0.020	0.245
RSG + Cement	0.30	0.020	0.040	0.050	0.020	0.130

*Chemically stabilized materials reported at 7 days of curing after first 10,000 cycles

Table 5.2. Summary Resilient Modulus (SM_R) and power model fitting parameters k_1 and k_2 (Eq. 2.2) for base materials.

Material	Test Method	Thickness (m)	Curing Time (d)	Measured Parameters		
				k_1	k_2	SM_R (MPa)
Class 5 gravel	Lab*	0.30	-	13.6	0.53	240
	LSME	0.20	-	19.7	0.53	280
		0.30	-	29.5	0.53	430
RPM	Lab*	0.30	-	49.2	0.34	310
	LSME	0.20	-	50	0.34	310
		0.30	-	82	0.34	510
RPM+4% C	Lab	0.30	28	19170	0	19170
	LSME	0.30	7	1240	0	1240
		0.30	28	1220	0	1220
RPM+10% CKD	Lab	0.30	28	5530	0	5530
	LSME	0.30	7	710	0	710
		0.30	28	1080	0	1080
RSG	Lab	0.30	-	21.6	0.44	230
	LSME	0.20	-	11	0.44	120
		0.30	-	20.6	0.44	220
RSG+4% C	Lab	0.30	28	21040	0	21040
	LSME	0.30	7	930	0	930
		0.30	28	1010	0	1010
RSG+10% CKD	Lab	0.30	28	37790	0	37790
	LSME	0.30	7	770	0	770
		0.30	28	1340	0	1340

Note: SM_R is calculated at a bulk stress of 208 kPa.
* Unstabilized Class 5 gravel and RPM reported by Camargo (2008). Lab results reported with internal LVDTs.

Table 5.3. Comparison of Laboratory Internal and External SM_R

Material	Internal SM_R (MPa)	External SM_R (MPa)	$SM_{R\ INT}/SM_{R\ EXT}$
Class 5 Gravel	240	170	1.4
RPM	310	220	1.4
RPM+4% C	19,170	330	58.1
RPM+10% CKD	5530	450	12.3
RSG	200	179	1.1
RSG+4% C	21,040	480	43.8
RSG+10% CKD	37790	790	47.8

Note: Unstabilized Class 5 gravel, RPM and RSG reported by Camargo (2008).

Table 5.4: Layer Coefficients and Structural Numbers of recycled materials

Material	Thickness (m)	SM_R (MPa)	Layer Coefficient, a	Structural Number, SN
Class 5 Gravel	0.20	280	0.17	1.34
	0.30	430	0.22	2.56
RPM	0.20	310	0.18	1.43
	0.30	510	0.24	2.78
RPM+4% C	0.30	1220	0.33	3.89
RPM+10% CKD	0.30	1080	0.32	3.74
RSG	0.20	120	0.08	0.62
	0.30	220	0.14	1.71
RSG+4% C	0.30	1010	0.31	3.65
RSG+10% CKD	0.30	1340	0.34	4.01

Note: SN calculated with English units of inches.

Table 5.5: Volume change of control specimens during durability testing

Test	Specimen	Cement CKD Content (%)	$V_{final}/V_{initial}$	Final Cycle
Freeze - Thaw	RSG + CKD	5	1.01	2
		10	1.15	5
		15	1.10	3
	RSG + Cement	3	1.06	12
		5	0.99	12
		7	1.00	12
	RPM + CKD	5	1.06	2
		10	1.05	2
		15	1.04	4
	RPM + Cement	3	1.06	12
		5	1.01	12
		7	0.97	12
Wet-Dry	RSG + CKD	5	1.07	3
		10	1.07	6
		15	1.12	4
	RSG + Cement	3	1.03	12
		5	0.99	12
		7	0.98	12
	RPM + CKD	5	1.01	12
		10	1.02	12
		15	1.00	12
	RPM + Cement	3	1.01	12
		5	0.96	12
		7	0.98	12

Note: Initial volume is based on the start of wet-dry or freeze-thaw cycling after 7 days of curing.

FIGURES

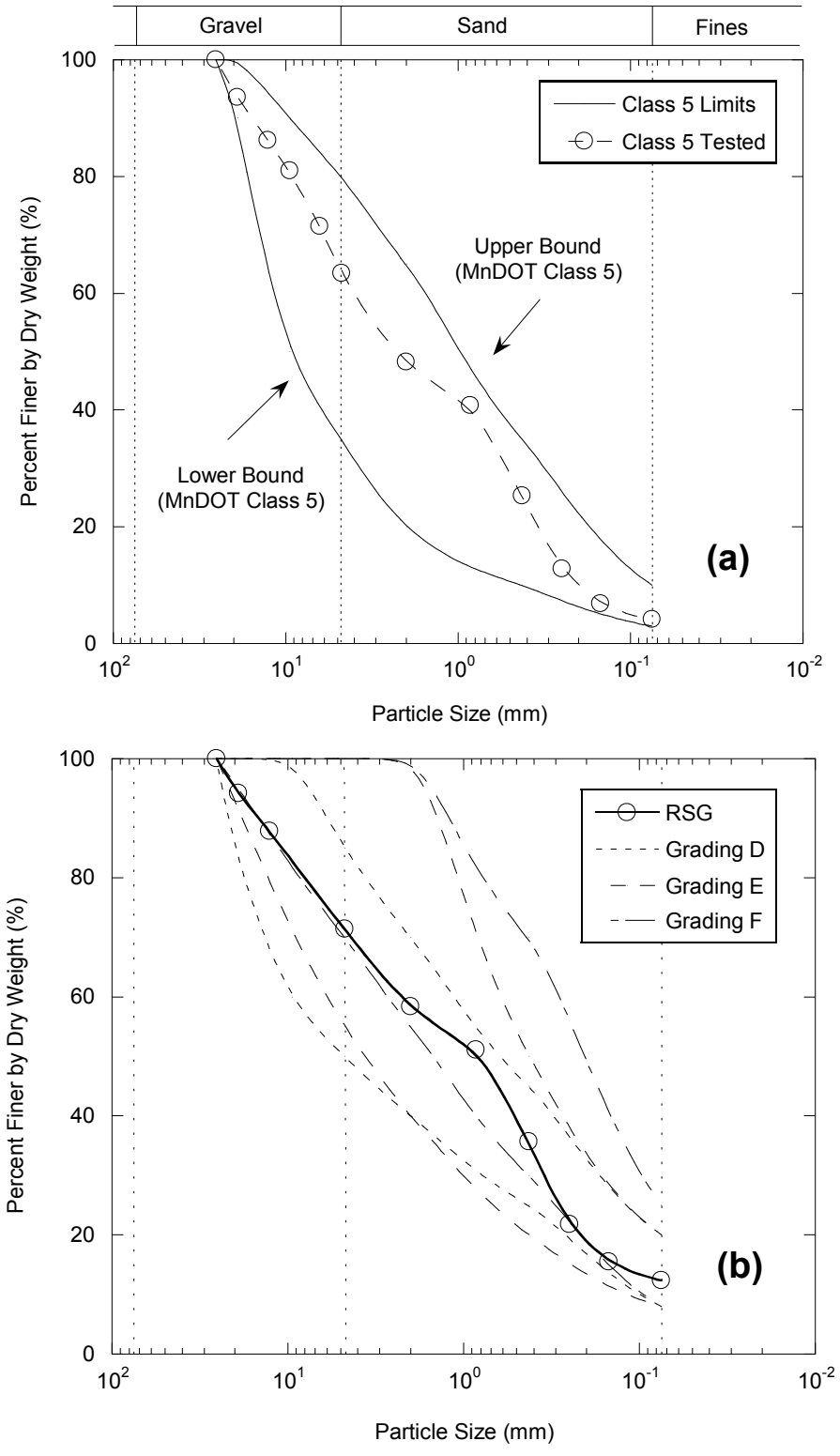

Fig. 3.1. Particle size distributions for (a) tested Class 5 base within MnDOT specifications (b) and RSG within AASHTO surface course specifications.

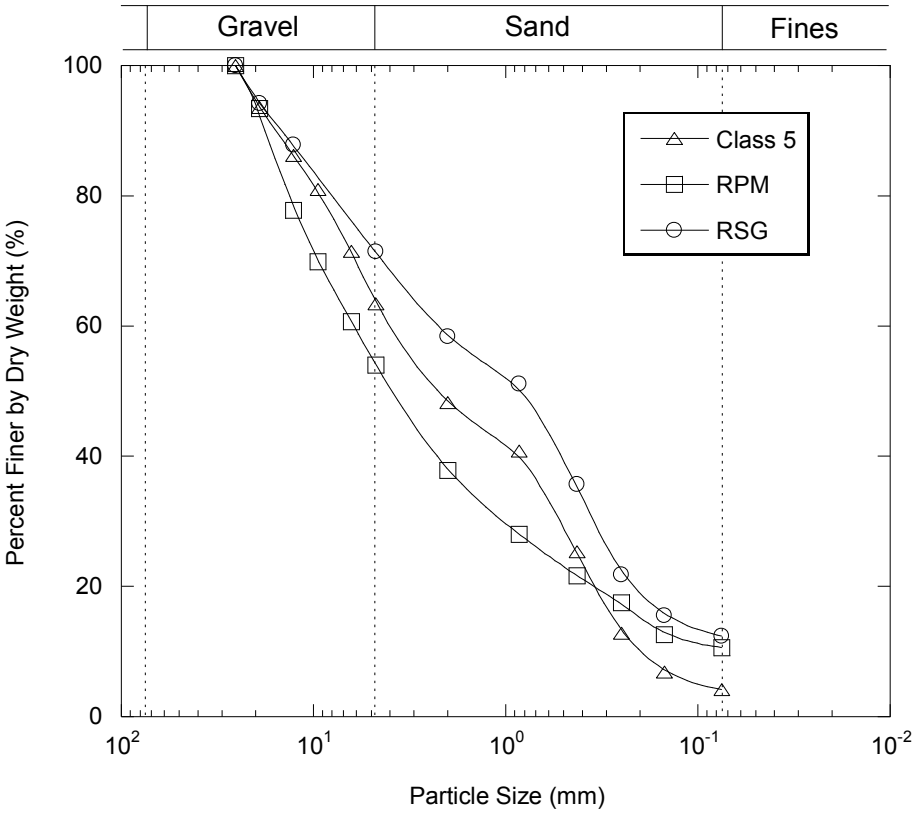

Fig. 3.2. Particle size distributions for Class 5 base, RPM, and RSG.

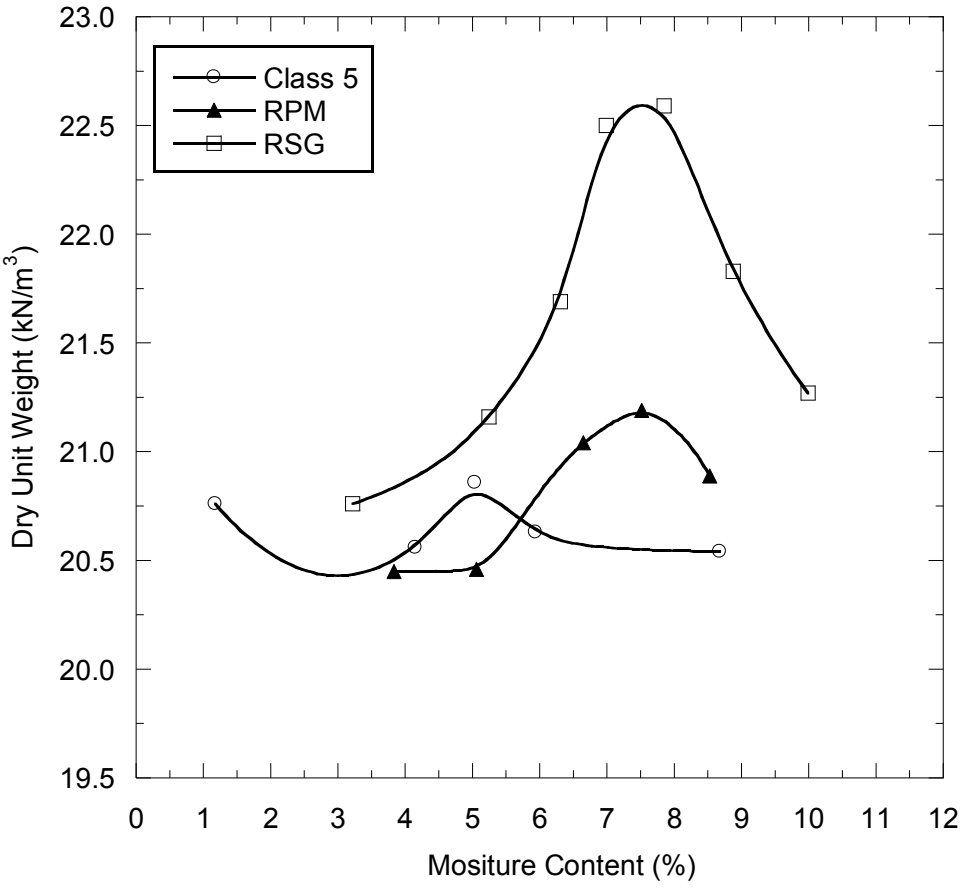

Fig. 3.3. Standard Proctor compaction curves for Class 5 base, RPM, and RSG.

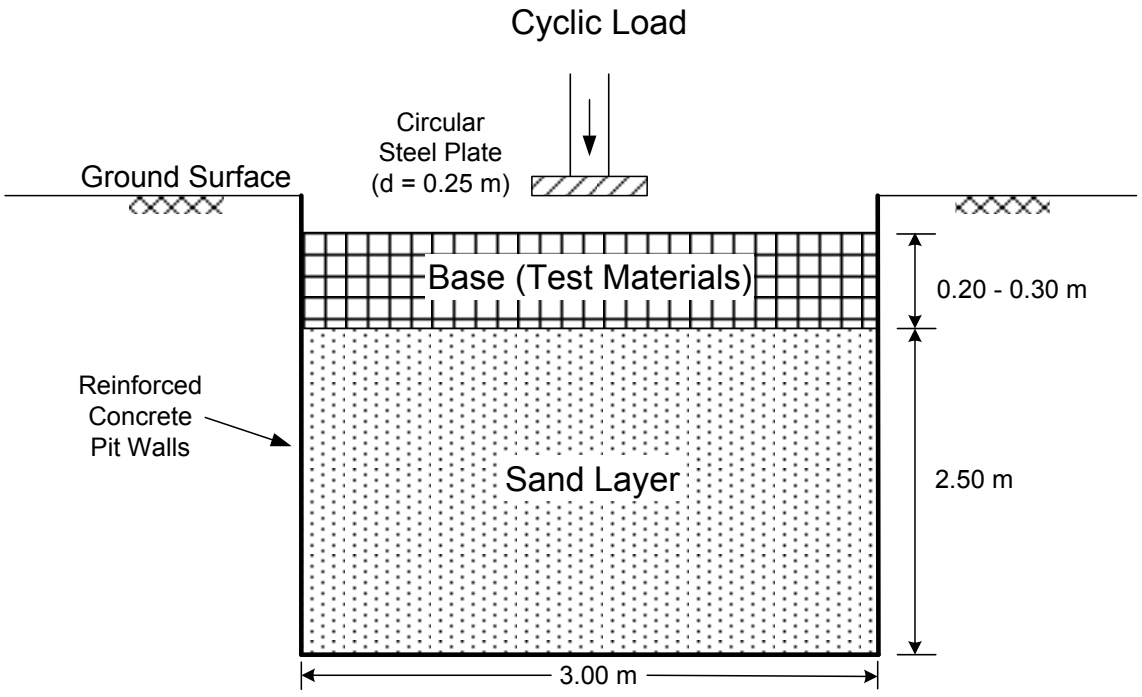

Fig. 4.1. Schematic cross section of Large-Scale Model Experiment.

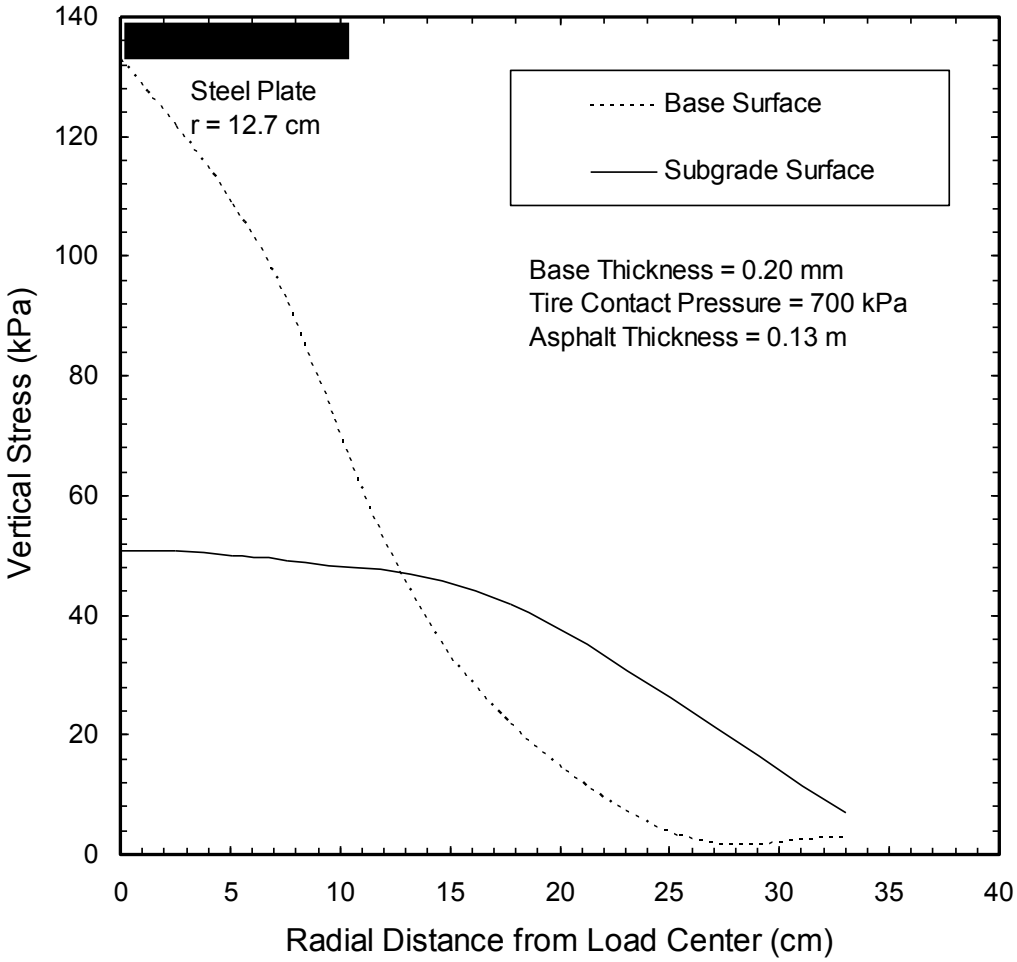

Fig. 4.2. Stress predicted by MICH-PAVE at the surface of a base course and subgrade layer at varying distances from the center of loading.

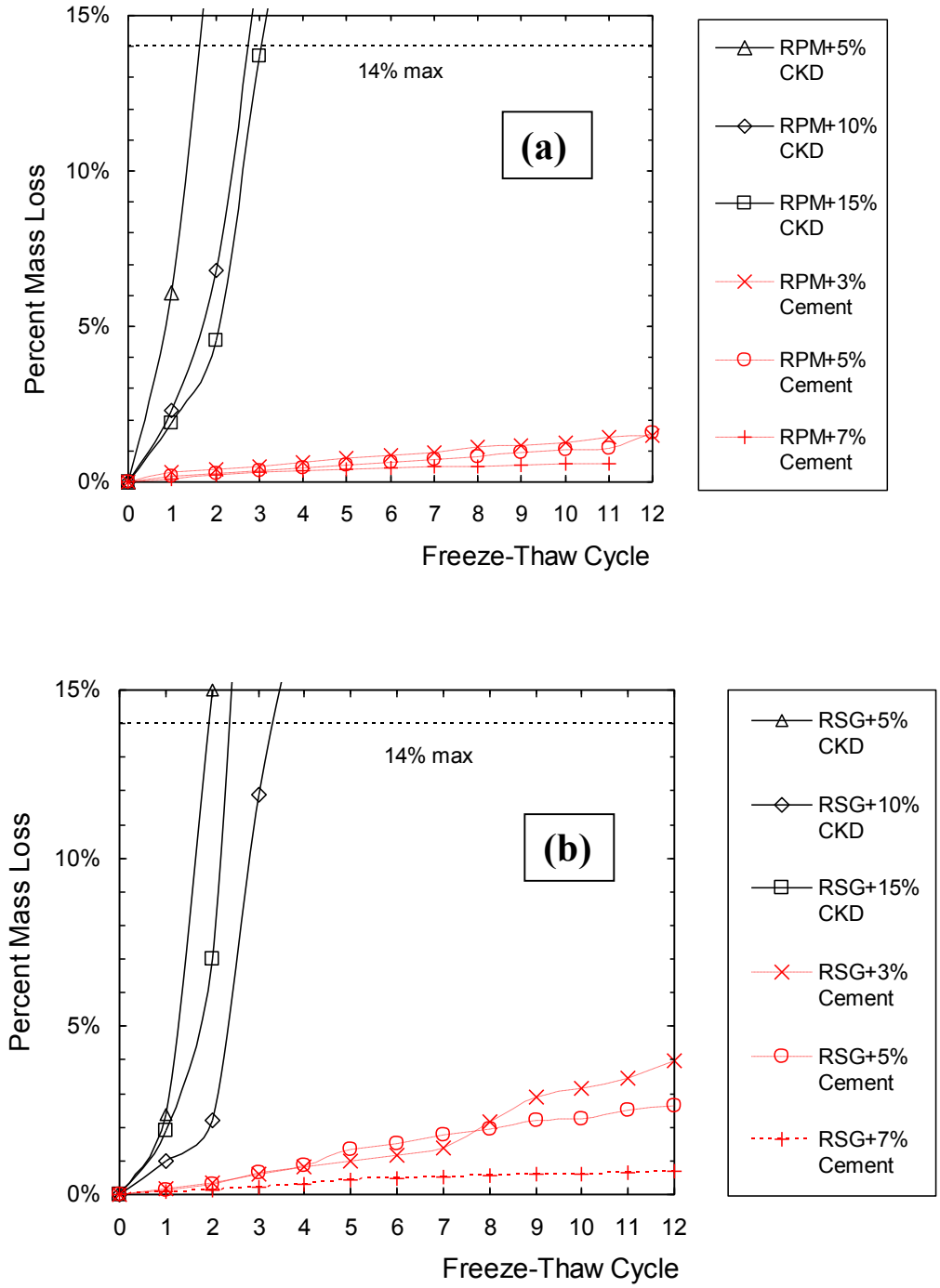

Fig. 5.1. Percent mass loss during freeze-thaw cycling for (a) RPM and (b) RSG blended with cement and CKD.

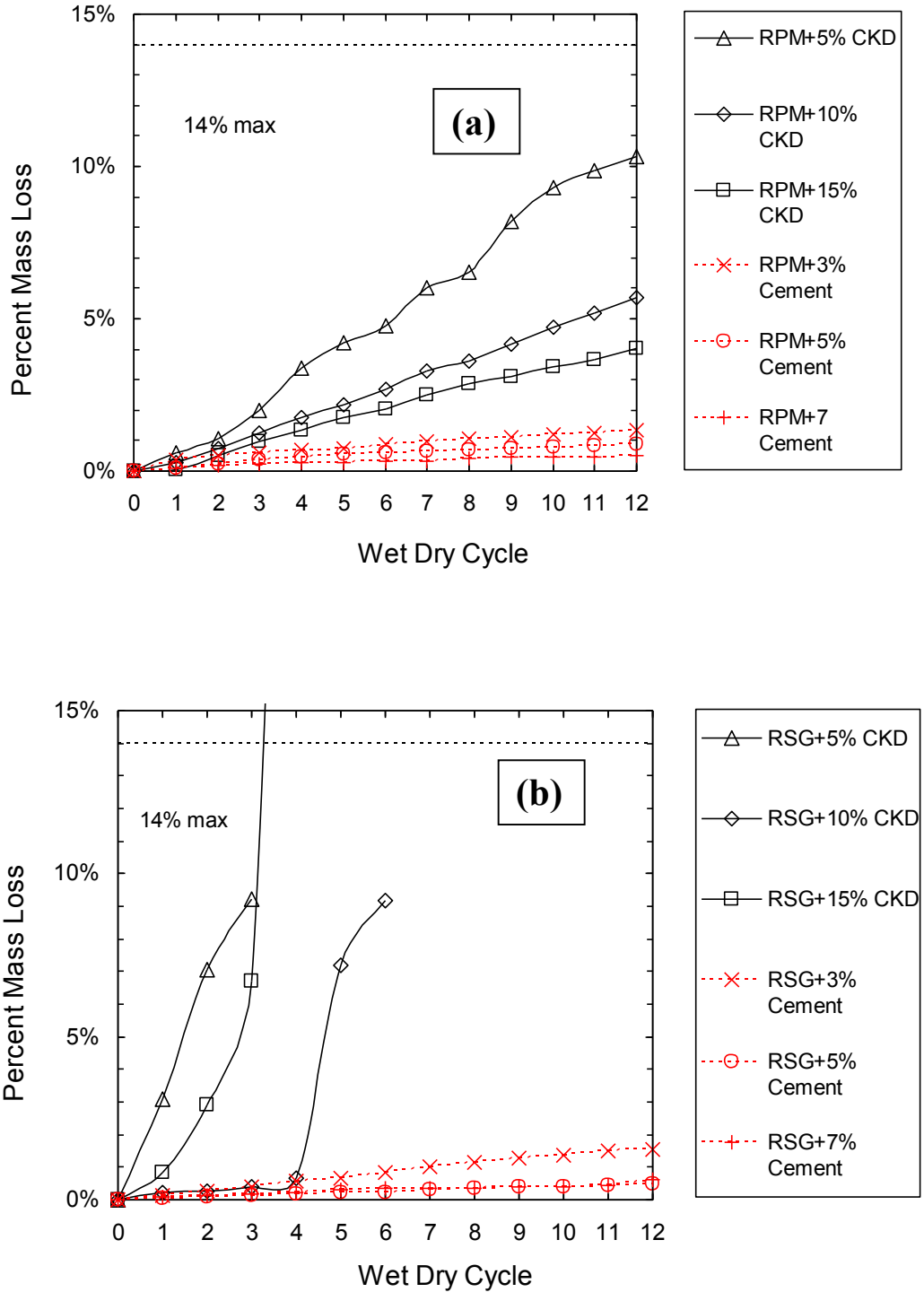

Fig. 5.2. Percent mass loss during wet-dry cycling for (a) RPM and (b) RSG blended with cement and CKD.

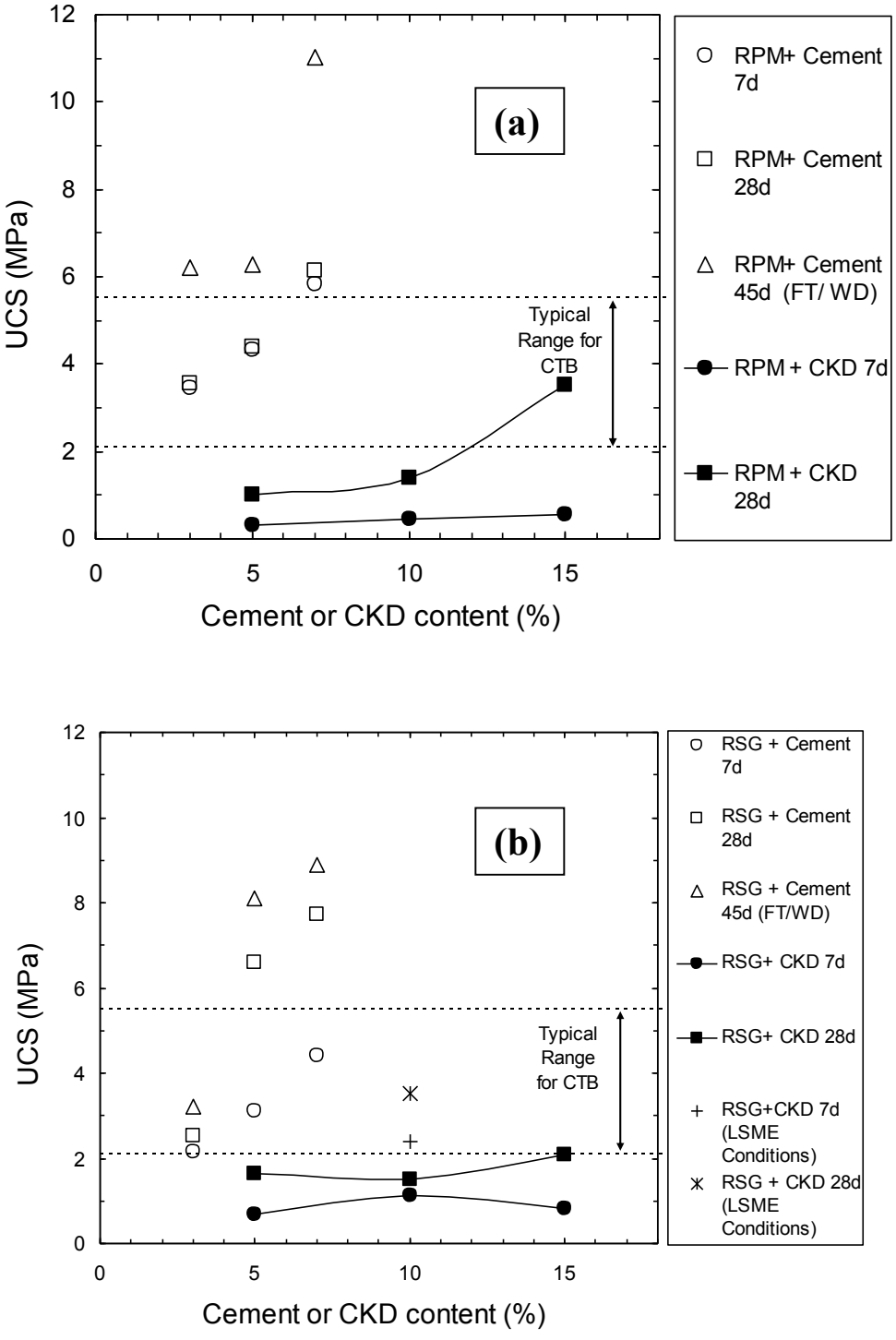

Fig. 5.3. Unconfined Compression Test results for (a) RPM and (b) RSG blended with cement and CKD.

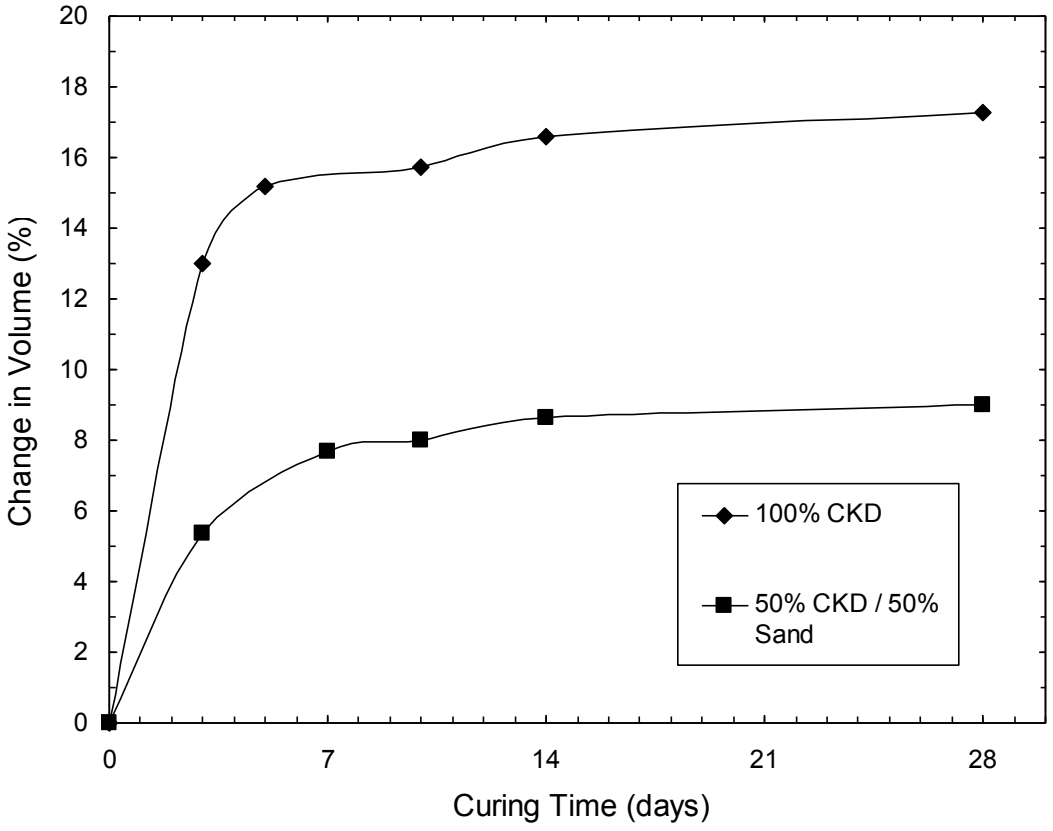

Fig. 5.4. Increase in volume during curing of CKD specimens.

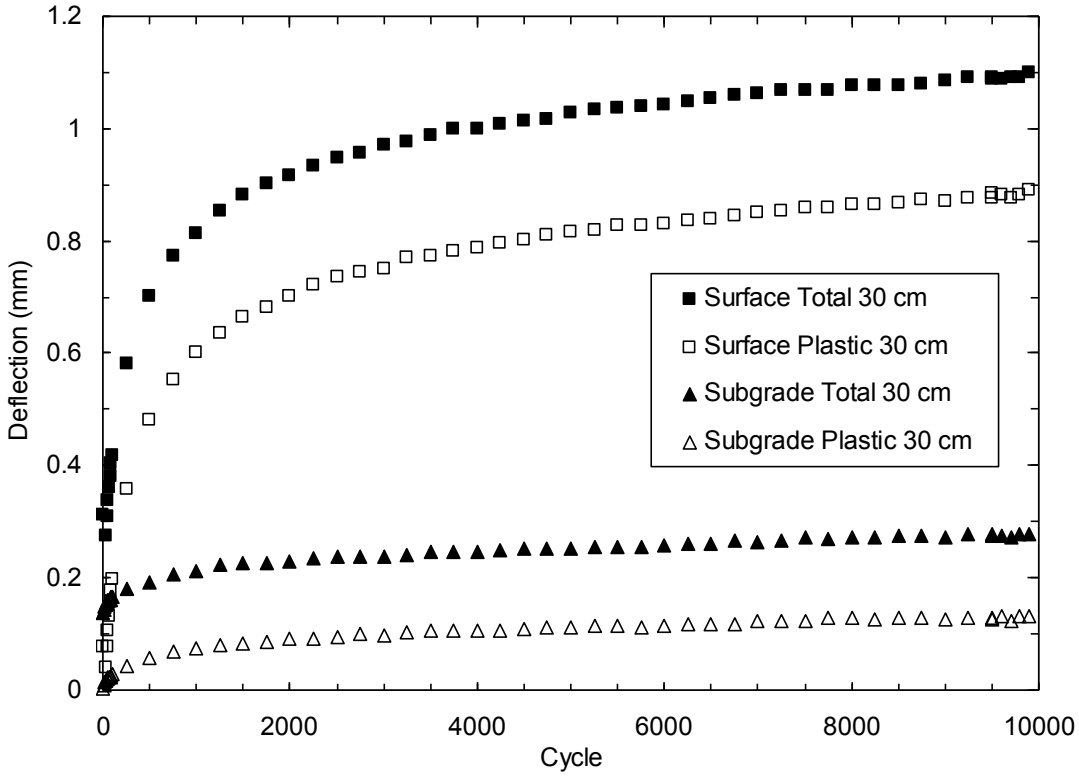

Fig. 5.5. Total deflection and plastic deformation at base and subgrade surfaces vs. number of load cycles for Class 5 gravel.

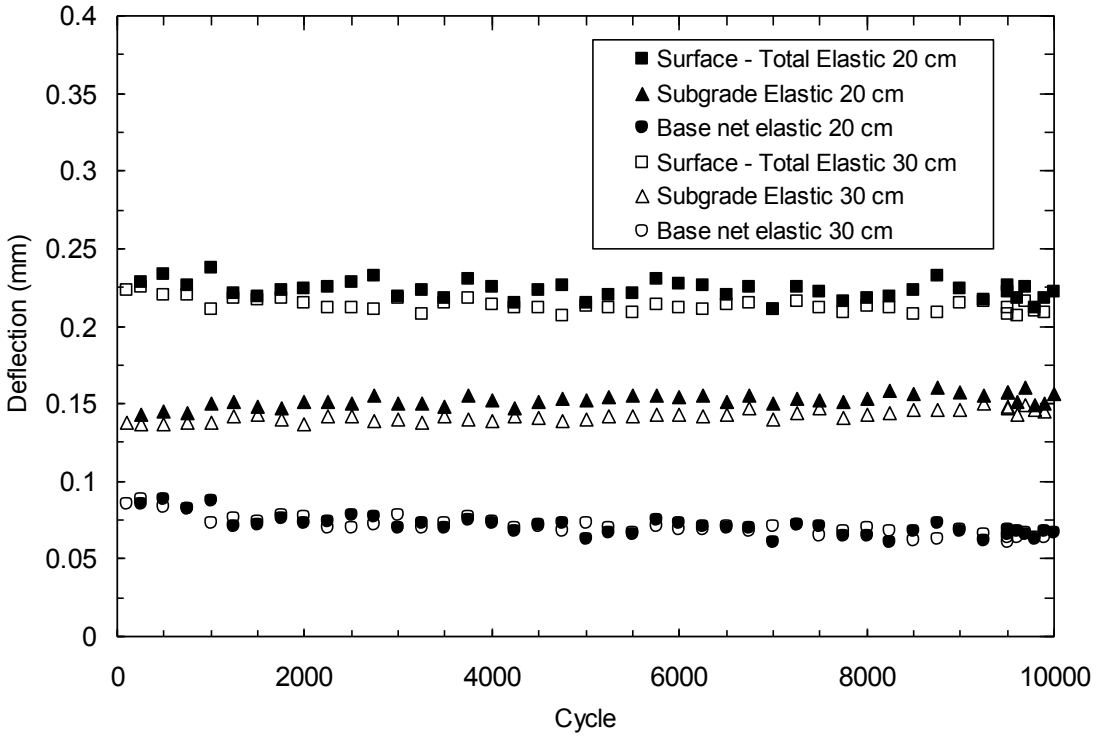

Fig. 5.6. Surface, subgrade and net base elastic deflections for 0.20 and 0.30 m thick layers of Class 5 gravel.

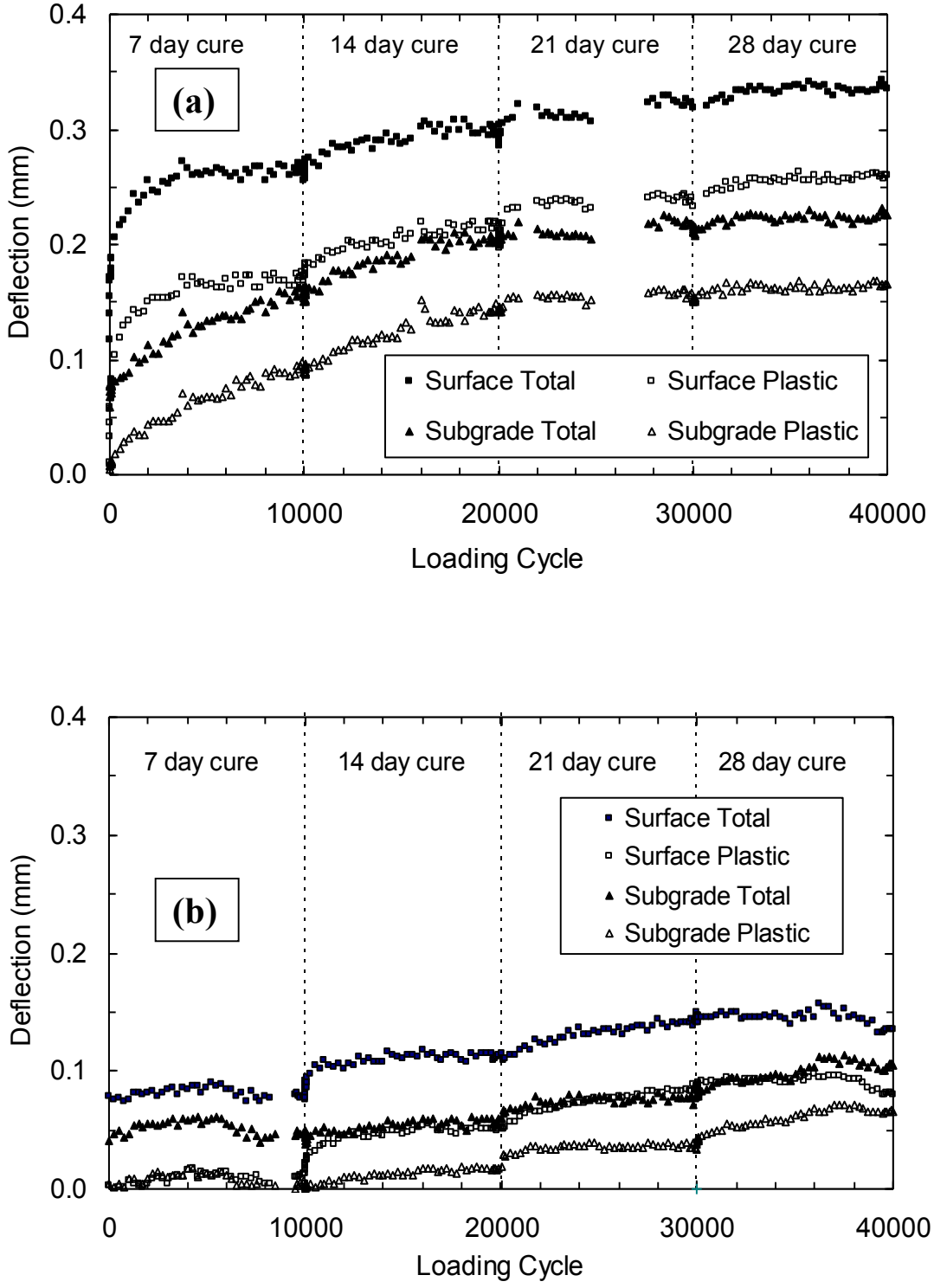

Fig. 5.7. Total deflection and plastic deformation vs. number of load cycles for (a) RPM and (b) RSG blended with CKD.

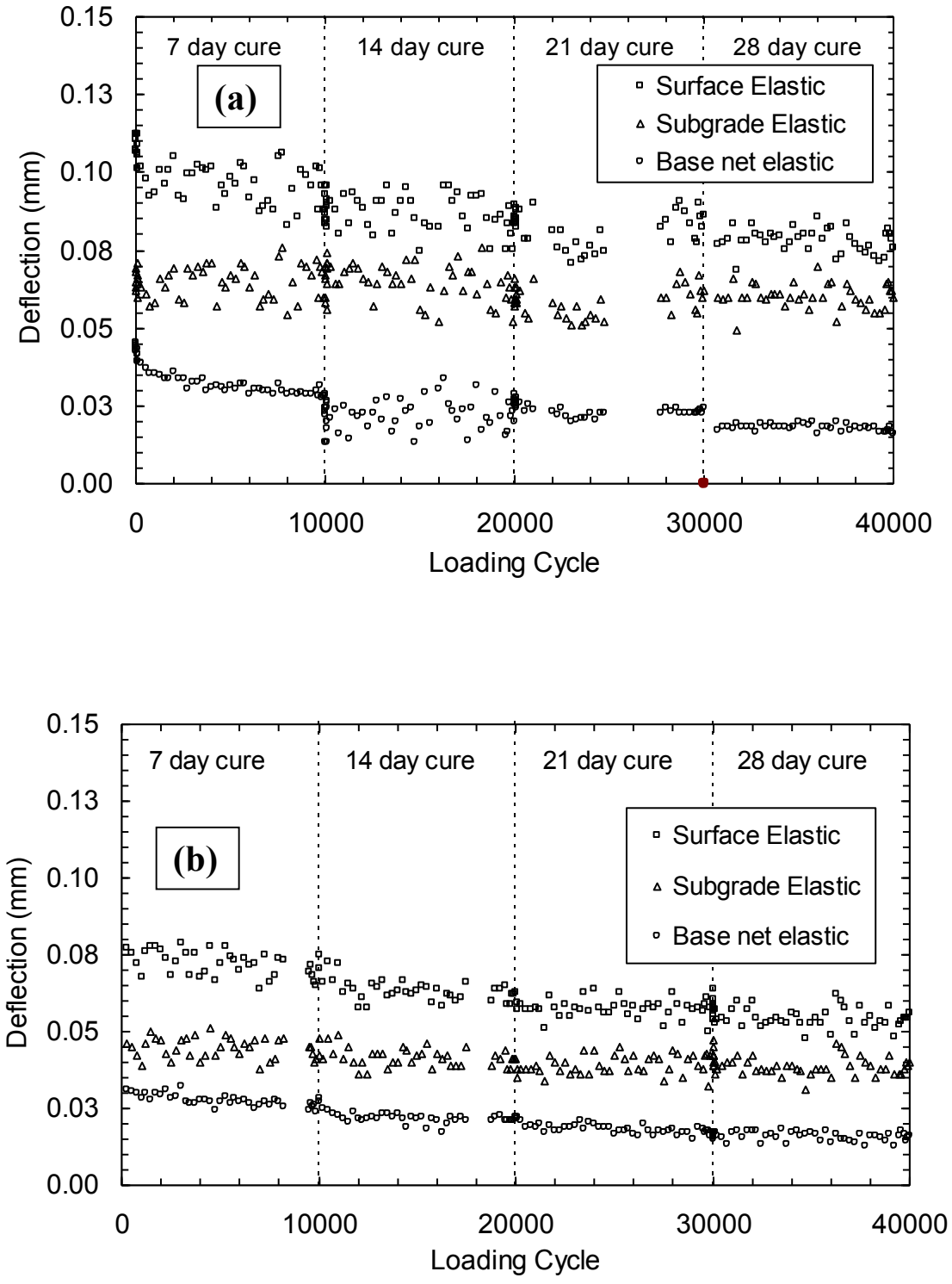

Fig. 5.8. Elastic deflections vs. number of load cycles for (a) RPM and (b) RSG blended with CKD.

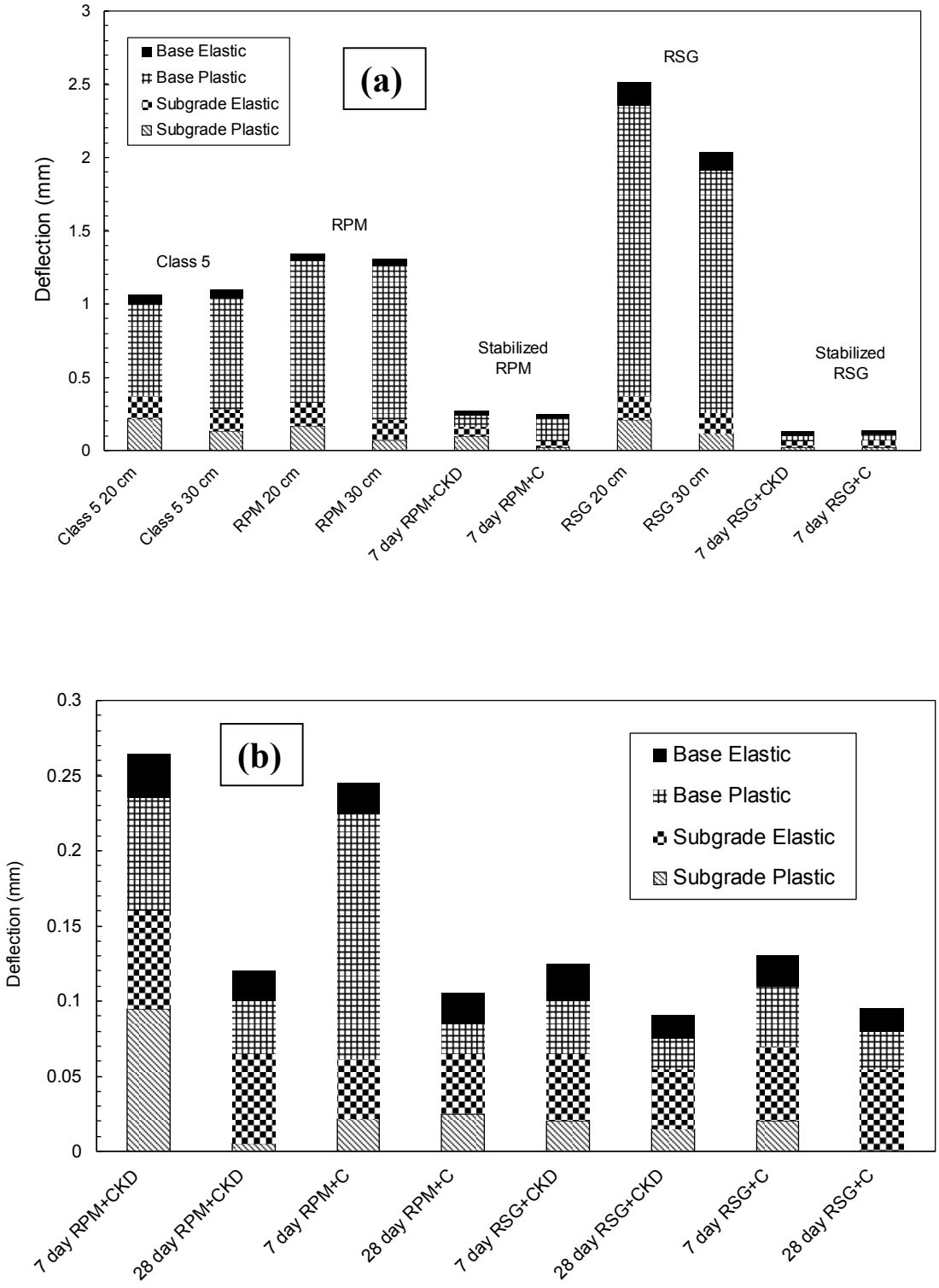

Fig. 5.9. Comparison of elastic deflection and plastic deformation measured in LSME between (a) unstabilized and stabilized material and (b) 7 and 28 day stabilized tests.

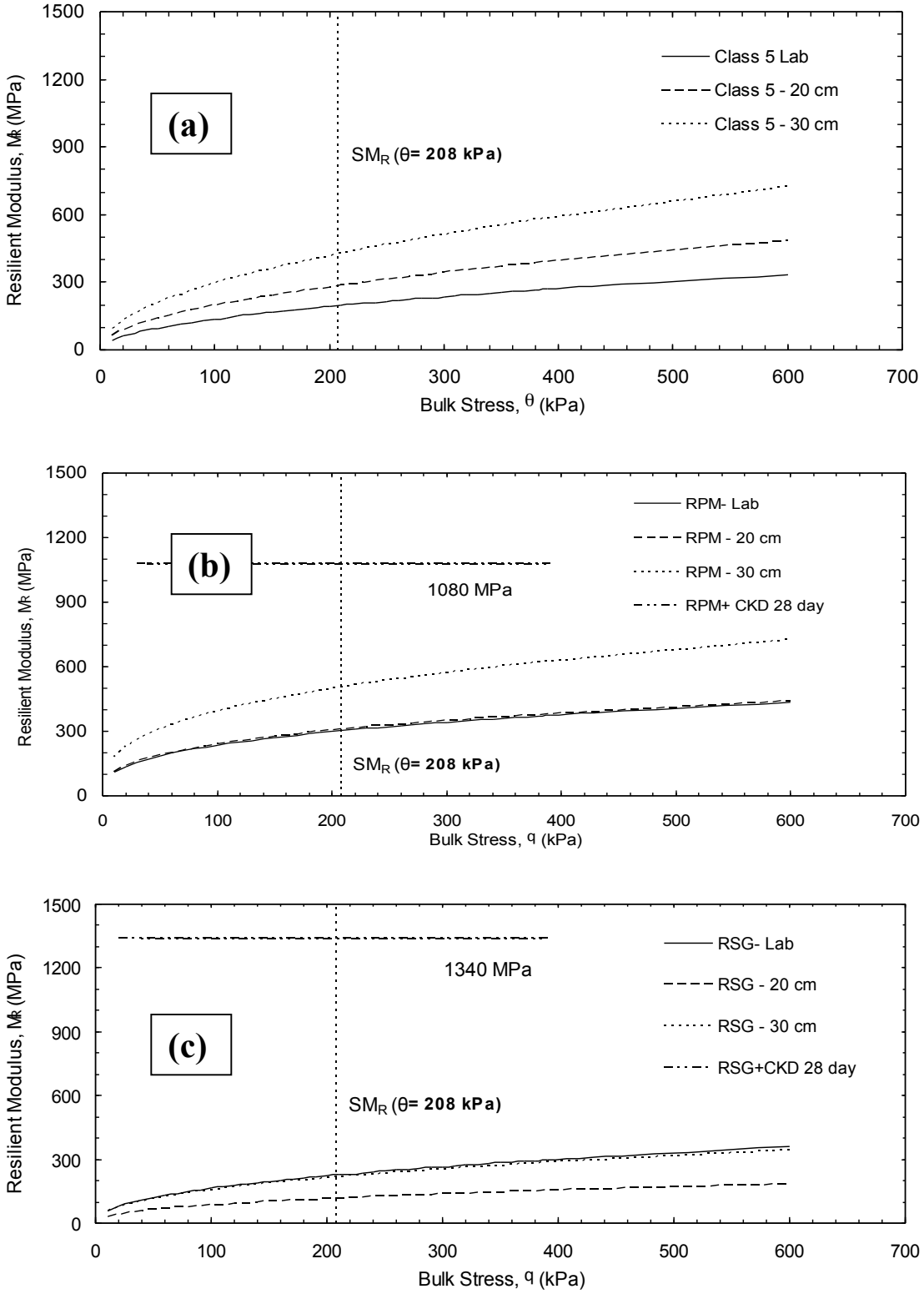

Fig. 5.10. Resilient modulus vs. bulk stress determined from LSME and laboratory tests (internal LVDTs) for (a) Class 5, (b) RPM, and (c) RSG.

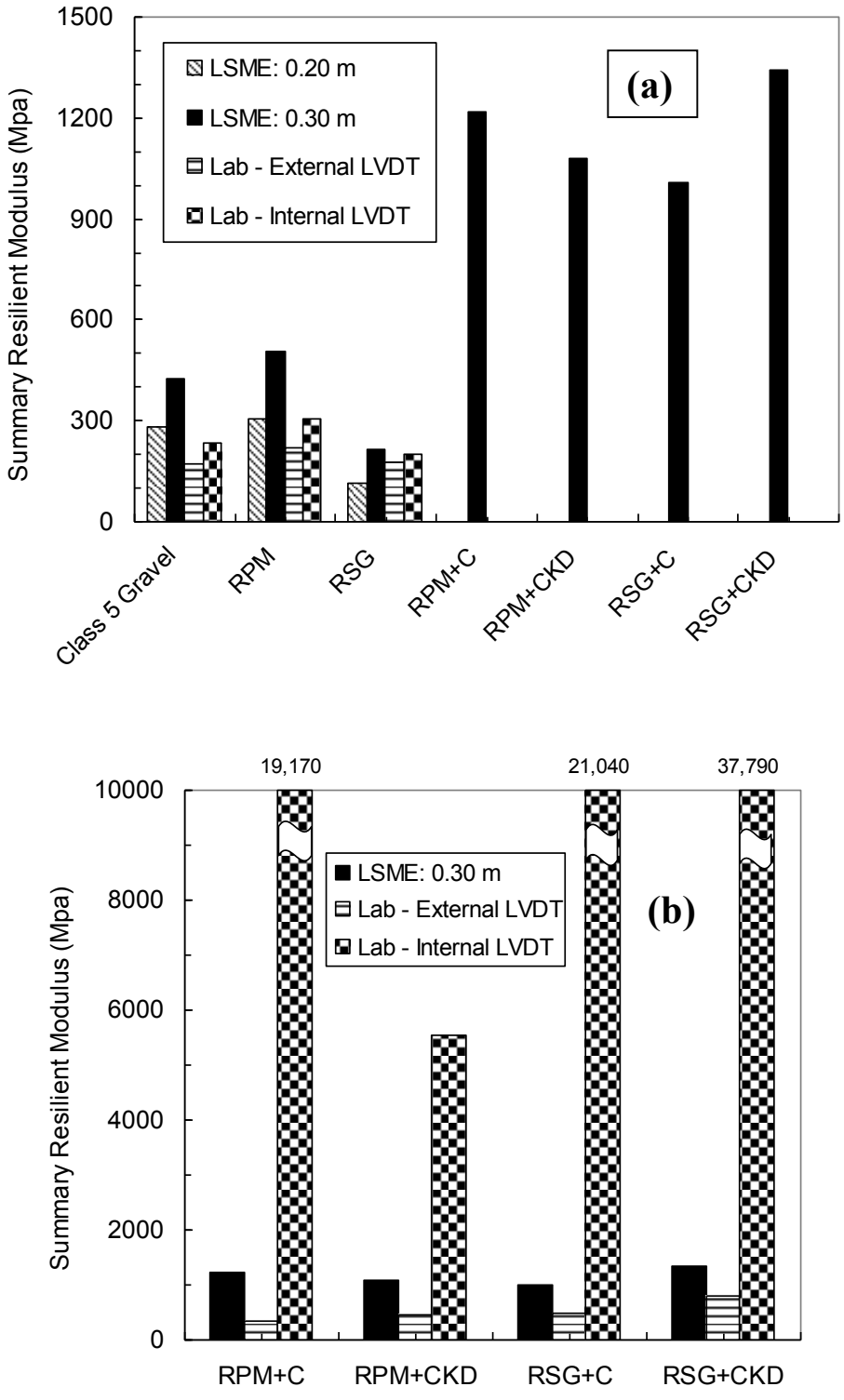

Fig. 5.11. Summary resilient modulus comparison of LSME and laboratory tests for (a) unstabilized with stabilized base and (b) stabilized with internal and external LVDTs. (Stabilized tests reported at 28 days of curing.)

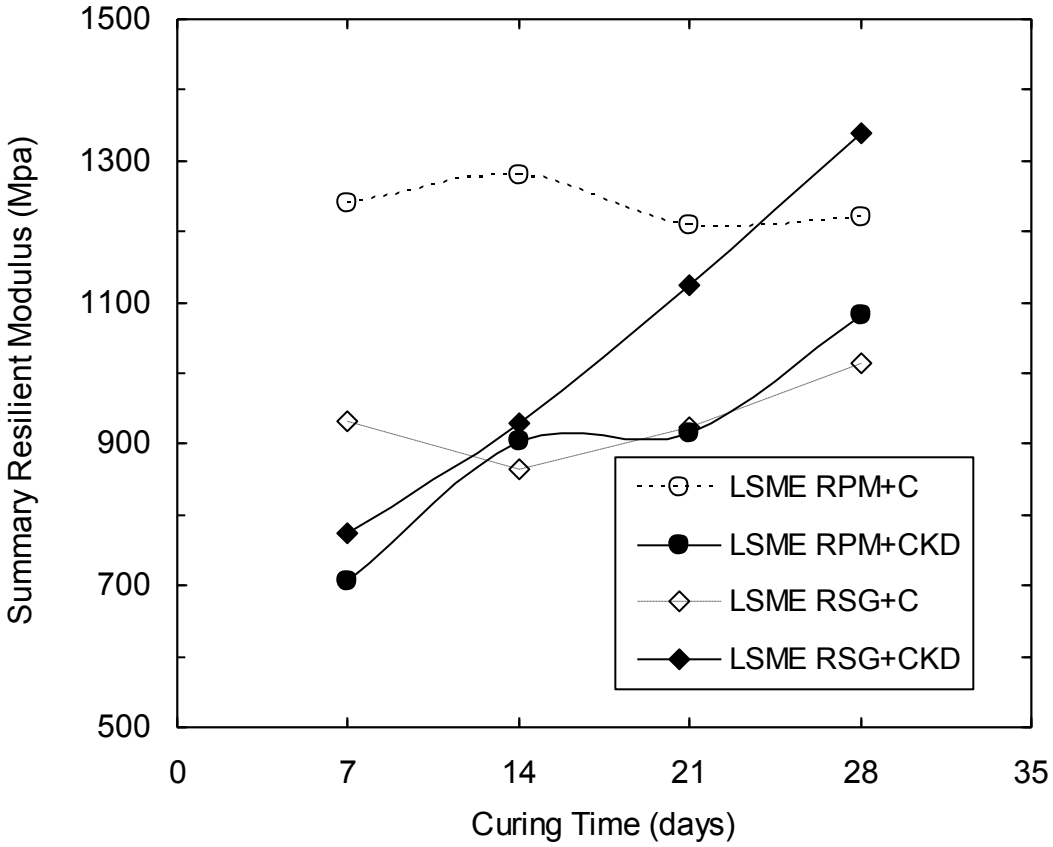

Fig. 5.12. Change of resilient modulus with curing time.

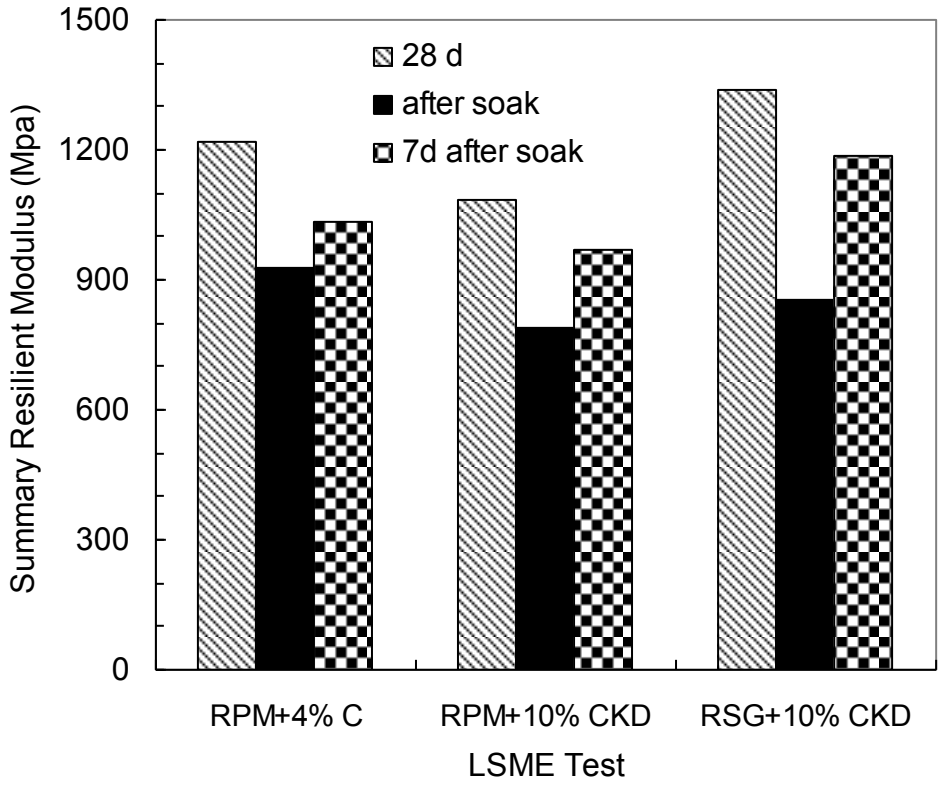

Fig. 5.13. Effect of soaking and drying on LSME resilient modulus.

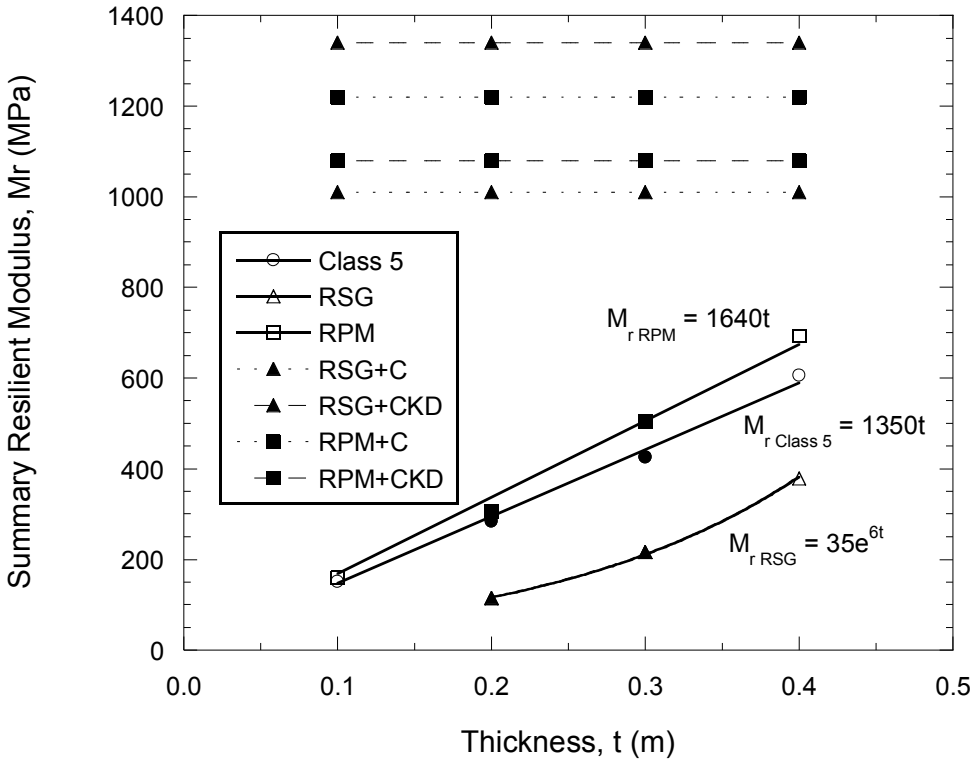

Fig. 5.14. Summary resilient modulus as a function of base layer thickness.

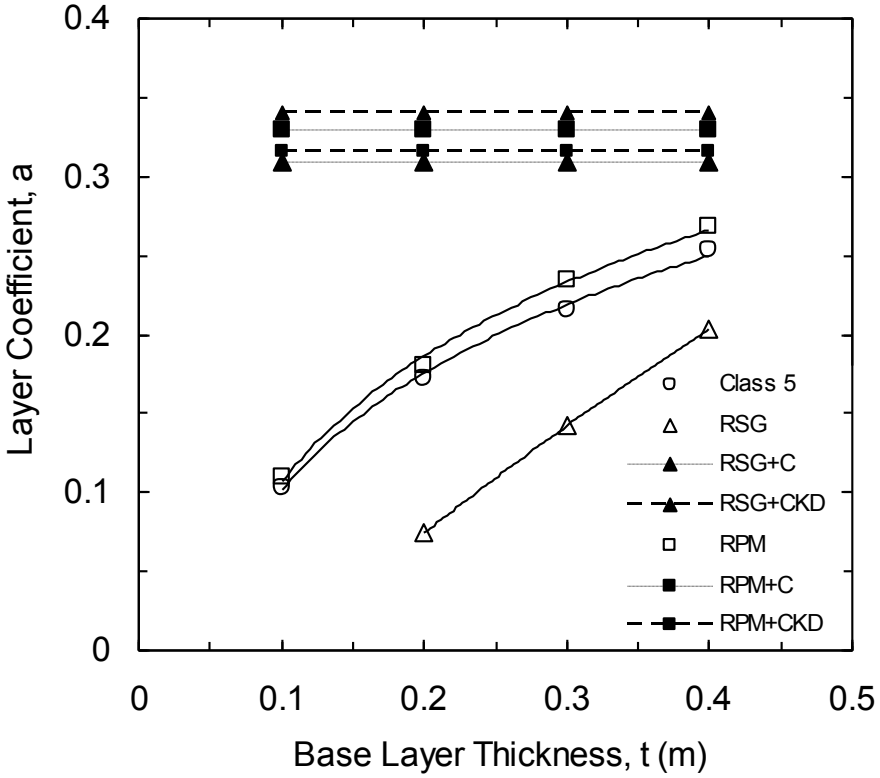

Fig. 5.15. Layer coefficient vs. base layer thickness

APPENDIX A: STRAIN DEPENDENCY OF MODULUS

A.1 INTRODUCTION

The unstabilized granular base course elastic modulus measured in the LSME is sensitive to the thickness of the layer being evaluated (i.e. thicker layers have a higher elastic modulus at a given bulk stress). This sensitivity of modulus to layer thickness reflects the varying levels of strain in the layers having different thicknesses, known to affect the elastic modulus of granular materials (Seed and Idriss, 1970, Hardin and Drnevich 1972, Edil and Luh 1978). Several studies have investigated the effect of strain level on modulus of layered pavement systems. Kim and Stokoe (1992) and Tanyu et al. (2003) demonstrated the effect of strain level on the resilient modulus of subgrade and various working platforms. Sawangsuriya et al. (2005) used the strain dependency of elastic modulus to predict the strain level of modulus with the soil stiffness gauge (SSG) for medium sand and crushed rock. Schuettpelz (2008) described the stress and strain dependency of modulus by finding a correlation between low strain elastic modulus (from seismic tests) and laboratory resilient modulus.

The strain-stress dependency of elastic modulus can be described with a backbone curve (Seed and Idriss, 1970, Hardin and Drnevich 1972). The backbone curve describes the ratio of shear modulus (or elastic modulus) at a given shear strain to the low strain shear modulus (or elastic modulus) as a function of shear strain. The relation between shear modulus and shear strain can be approximated with a hyperbolic function:

$$\frac{G}{G_{max}} = \frac{1}{1+\gamma_h} \tag{A.1}$$

where Hardin and Drnevich refer to γ_h as the hyperbolic strain. The hyperbolic strain is the strain normalized with respect to the reference strain (γ_r):

$$\gamma_h = \frac{\gamma}{\gamma_r}\left[1 + ae^{-b\left(\frac{\gamma}{\gamma_r}\right)}\right] \quad \text{(A.2)}$$

where a and b describe the shape of the backbone curve. The reference strain is defined as the strain at the intersection of maximum shear stress and shear modulus (Hardin and Drnevich 1972)

Different test equipment and methods result in various stress and strain levels, so both strain dependency and stress levels are taken into account in comparing the modulus provided from different test methods and materials.

Kokusho (1980) examined some of the properties affecting modulus including confining stress. Modulus increases with confining pressure because the soil deforms less with the increased confinement of particles. A higher modulus is expected with a higher confining pressure while the strain level remains constant.

To consider the effect of confining pressure on the modulus, low strain modulus was measured at different bulk stresses by means of seismic tests. The predicted modulus of the material from MICH-PAVE was normalized with the low strain modulus for a specific bulk stress.

A.2 MEASUREMENT OF MAXIMUM (LOW STRAIN) MODULUS

A.2.1 Micro-Electro-Mechanical Systems (MEMS) Accelerometers.

Small MEMS accelerometers were used to measure low strain modulus (maximum modulus) of different materials in the LSME. The accelerometers measure particle accelerations caused by a propagating elastic wave as it travels vertically through soil, and also measure horizontal and vertical components of the acceleration caused by the gravitational field.

The MEMS accelerometers used were Analog Devices ADXL 203CE dual axis MEMS having a sensitivity of 1000 mV/g up to 1.5 g, were 4 mm x 4 mm x 1.5 mm in size and sensitive to both static (e.g., gravity) and dynamic (e.g., vibration) accelerations. The corresponding 18 mm by 18 mm printed circuit boards (PCB) manufactured by Sparkfun Electronics are shown in Fig. A.1. Each printed circuit board contains 0.1 μF filtering capacitors and a 1 MΩ resistor required for operation.

Four to six accelerometers (depending on layer thickness) were used to measure change of velocity with depth using the elastic wave arrival time in the LSME. The use of small MEMS accelerometers spaced a few centimeters apart allows the detection of small changes in velocity similar to the way that geophones can detect these changes on the order of meters and kilometers in field scale seismic studies (Schuettpelz, 2008). Although MEMS accelerometers can be used on a scale of centimeters, great care must be taken to ensure precise measurement of the distance between accelerometers. A small change in the separation distance between accelerometers can produce a large change in the calculated velocity leading to unreliable results.

Prior to placing each accelerometer in the soil layer, they were first coated with a durable, water tight epoxy seal (Fig. A.2). The seal not only ensures that water or dust will not shortcut the electronic components of the system, but also mechanically protects the fragile accelerometer, PCB, and wires. When several accelerometers are situated a known distance apart, the velocity of a propagating elastic wave can be calculated by choosing the arrival time of the elastic waves in the soil.

A.2.2. Elastic Wave Velocity Measurement with MEMS Accelerometers.

MEMS accelerometers were used to measure the dynamic response of the accelerometer to the propagation of an elastic wave generated by hitting the LSME loading plate with a hammer. As the elastic wave progresses into the soil the

acceleration changes and the arrival time of the elastic wave can be captured for each accelerometer. The velocity of an elastic primary (V_p) or shear (V_s) wave can be calculated knowing the arrival time of the wave at each accelerometer and the distance between accelerometers (50 mm in this study). The elastic wave propagation through RSG is shown in Fig. A.3. The first arrival time was determined manually by extending the most linear portion of the wave form to the x-axis. Although the accelerometers are equipped to measure two components of vertical and horizontal acceleration, only the vertical component is necessary to compute the elastic wave velocity.

V_p in particulate media is dependent on the elastic modulus (E), Poisson's ratio (ν) and density (ρ) (Santamarina et al. 2001; Richart et al. 1970):

$$V_p = \sqrt{\frac{E(1-\nu)}{\rho(1+\nu)(1-2\nu)}} \tag{A.3}$$

The velocity of wave propagation increases with increasing applied load and soil stiffness. By rearranging Eqn. A.3, low strain elastic modulus can be calculated from V_p measured in seismic tests, along with ρ and ν of the material:

$$E_s = \frac{V_p^2 \rho(1+\nu)(1-2\nu)}{(1-\nu)} \tag{A.4}$$

where ν was considered to be 0.35 for the unstabilized materials and 0.20 for stabilized RPM and RSG. The constitutive relationship between bulk stress and E_s for the base course materials evaluated is shown in Fig. A.4, where Class 5 gravel has the lowest E_s and RPM has the greatest E_s among the unstabilized materials. RPM results in the greatest E_s of the three unstabilized base courses, consistent with RPM having the greatest M_R from LSME and laboratory (NCHRP 1-28) test results. The seismic test resulted in Class 5 gravel having the lowest E_s, whereas RSG was shown to have the lowest M_R in LSME and laboratory tests. The higher E_s of RSG compared with Class 5 is likely due to the effect of P-wave velocities within the pore water of RSG which was

compacted at a higher optimum water content than Class 5. The stress dependency of unbound granular materials can be described with Hertz contact theory (1971) where the relationship between force and displacement in particulate media is non-linear. As grain boundary contact areas continue to flatten with more applied force, the amount of deformation in the form of displacement over the soil column decreases. A decrease in deformation as force increases results in an increased stiffness of soil.

Chemically stabilized materials, such as those blended with fly ash, showed a constant modulus in the applied range of stress. The stress independency of modulus for these materials is attributed to cementation binding the soil particles together.

A.3. STRESS-STRAIN DEPENDENCY OF MODULUS (BACKBONE CURVE)

The backbone curve as described in the introduction of this Appendix was developed with shear strain on the horizontal axis and normalized resilient modulus at various bulk stresses on the vertical axis. MICH-PAVE was used to back-calculate the resilient modulus, along with vertical stresses and strains within a base course layer from data collected in the LSME. Shear strain was obtained from the back-calculated vertical strain (Kim and Stokoe, 1992; Tanyu, 2003):

$$\gamma = \varepsilon\,(1+\nu) \tag{A.5}$$

where γ is the shear strain, ε is the vertical strain, and ν is Poisson's ratio. The normalized resilient modulus was determined using Eqn. A.6:

$$\text{Normalized resilient modulus} = \frac{M_R}{E_s} \tag{A.6}$$

where M_R is the predicted resilient modulus for a particular bulk stress using Eqn 2.2, and E_s is the low strain elastic modulus determined from seismic tests for the same bulk stress obtained from Fig. A.4. The parameters a and b in Eqn. A.2 were adjusted to obtain a best fit to the calculated points. Care should be taken when using the results of

seismic tests to normalize the resilient modulus. Scatter of the data, specifically at low bulk stresses, can be misleading when evaluating the proper low strain elastic modulus used to normalize the resilient modulus.

The resulting backbone curves showing normalized modulus as a function of shear strain are shown in Fig. A.5 for the three unbound base course materials tested. The backbone shape describes the stress-strain behavior of the base material being evaluated and is unique for each material. The results of back-calculated LSME tests for different thicknesses and laboratory resilient modulus tests (NCHRP 1-28A) are placed together on the backbone curves, which are also summarized in Table A.1. Fig. A.5 shows that the LSME generally produces smaller strain levels than the laboratory resilient modulus test. Therefore the strain level in the base course of a full-scale pavement system may be smaller than strain levels produced in laboratory resilient modulus tests, and therefore resulting in a higher resilient modulus. The change of strain level in thicker material was evaluated by the means of backbone curves, and a smaller strain level can be seen in a thicker base course layer of 0.3 m as compared to a 0.2 m thick layer due to greater stress distribution within the thicker layer.

No stress dependency was observed for the materials mixed with fly ash as shown in Fig. A.4 and confirmed by the results of laboratory resilient modulus tests, where k_2 in Eqn. 2.2 was found to equal 0. To verify the effect of strain and stress level on the modulus of the materials blended with fly ash in the LSME, several tests were performed with different applied load levels corresponding to different strain levels. The results showed no stress and strain dependency of modulus for the materials cemented with fly ash in a range of applied stress and strain considered to be typical of the load from vehicle tires transferred to the base course in a pavement system (Fig. A.6).

A.4. PREDICTING BASE LAYER RESILIENT MODULUS FOR VARIOUS THICKNESSES OF BASE COURSE MATERIAL

In addition to comparing the results of LSME and laboratory tests based on strain level, backbone curves were used to extrapolate the modulus for other thicknesses not evaluated in this study. Since LSME tests are time consuming and labor intensive to perform, the ability to predict M_R of different materials over a range of thicknesses would aid in using M_R to determine the AASHTO layer coefficient or the gravel equivalency (GE) in pavement thickness design. Effects of strain and stress levels should be taken into account in predicting the base M_R for thicknesses not tested in the LSME.

LSME tests were conducted on RPM, RSG and Class 5 gravel in thicknesses of 200 and 300 mm. LSME test results for these base materials are shown in Fig. A.7, where base layer thickness is located on the horizontal axis and the summary resilient modulus (SM_R) at a bulk stress of 208 kPa is located on the vertical axis. Resilient modulus increases with increasing layer thickness due to changes of strain and stress levels within the soil layer. As material thicknesses increase under a constant load, deflections decrease due to the lower strain levels throughout the layer, resulting in a higher M_R.

The method used to predict M_R based on base layer thickness is demonstrated with the RPM results, and can also be used for the Class 5 gravel or RSG. MICH-PAVE was used to model the nonlinear elastic behavior of a two-layered system consisting of a base course over a subgrade material with the stress-dependent modulus function (Eqn. 2.2). The assumption was made that k_2 would not vary with thickness. The subgrade was considered to be linearly elastic with a modulus of 70 MPa determined from all LSME tests by averaging backcalculated subgrade moduli. The applied load of 7.3 kN was the same used in all LSME tests.

Various trials were conducted with MICH-PAVE to determine the appropriate k_1 parameter, and therefore SM_R, by assuming a k_1 and calculating the resulting shear

strain and normalized resilient modulus to be plotted with the backbone curve. A trial and error procedure was carried out by changing k_1 until the resulting shear strain and normalized resilient modulus resulted in a point located on or very near the backbone curve developed from the actual LSME test results described previously.

For example, the first trial with RPM consisted of a 450 mm thick layer. MICH-PAVE predicted the stresses and strains based on an assumed k_1 from which shear strains and normalized moduli were calculated. The first trial corresponding to a calculated SM_R of 570 MPa is compared to the RPM backbone curve as shown in Fig. A.8. The predicted data did not fit properly on the RPM backbone curve for the assumed k_1 so additional attempts were made to find a better fit to the backbone curve for the 450 mm thick layer of RPM. Additional trials were conducted by changing k_1, shown in Fig. A.8. The SM_R corresponding to the best backbone fit of 450 mm thick RPM was 768 MPa.

The results of predictions for several typical RPM thicknesses used in road construction are shown on the backbone curve in Fig A.9, along with the actual thicknesses tested in the LSME. The predicted SM_R for a range of RPM thicknesses are shown in Fig. A.10, along with the backcalculated SM_R for thicknesses tested in the LSME. The variation of modulus as a function of thickness is expected to level off for thicknesses greater than 550 mm because the normalized modulus enters the nonlinear section of the backbone curve corresponding to very low strains. The same procedure was performed for Class 5 gravel and RSG, and the results are included in Fig. A.10. This graph could easily be used by a pavement designer to select an appropriate value of resilient modulus of a pavement material for use in various pavement thickness design methods.

Table A.1. Summary resilient modulus and low strain elastic modulus used to develop the backbone curve

Material	test	Bulk stress (θ)	Low strain modulus E_s	SM_R[1]	Normalized modulus M_R / E_s	Shear strain (γ)
Class 5	Lab (NCHRP 1-28)	100-800	600-800	130-460	0.16-0.25	5-10 x 10^{-4}
	LSME 200 mm	81-207	500-800	180-280	0.37	4.5 x 10^{-4}
	LSME 300 mm	45-175	320-750	195-400	0.58	2.5 x 10^{-4}
RPM	Lab (NCHRP 1-28)	100-500	1000-1400	150-400	0.21-0.30	1.5-4 x 10^{-4}
	LSME 200 mm	70-220	900-1300	200-300	0.24	3 x 10^{-4}
	LSME 300 mm	40-180	700-1450	280-500	0.38	2 x 10^{-4}
RSG	Lab (NCHRP 1-28)	100-600	500-1000	130-500	0.28-0.35	3-7 x 10^{-4}
	LSME 200 mm	90-250	540-980	80-130	0.15	10^{-3}
	LSME 300 mm	70-220	400-800	130-230	0.29	5 x 10^{-4}

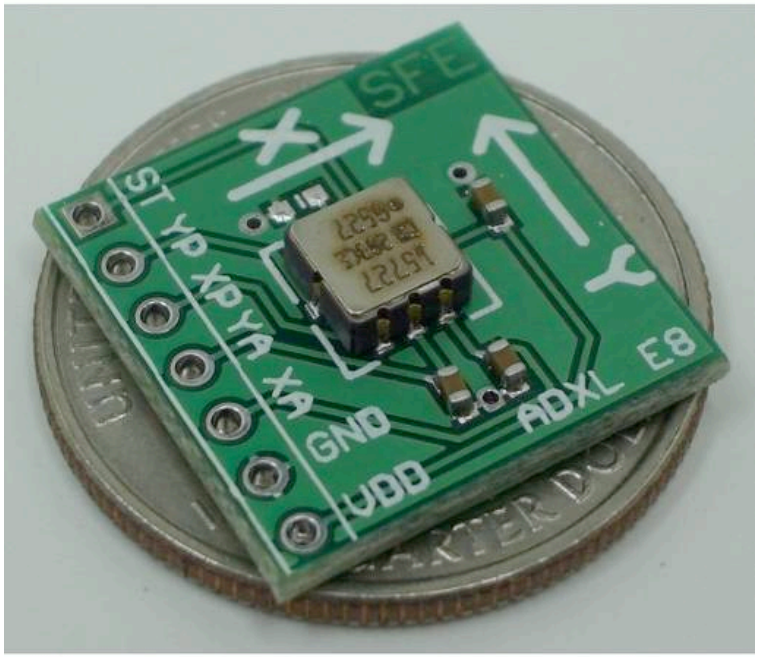

Fig. A.1. Analog Devices ADXL 203CE accelerometer and corresponding printed circ board (PCB, Sparkfun Electronics), (adopted from Schuettpelz, 2008).

Fig. A.2. Smoothcast 327 coating applied to MEM accelerometer and PCB (ruler gradations are in cm), (adopted from Schuettpelz, 2008).

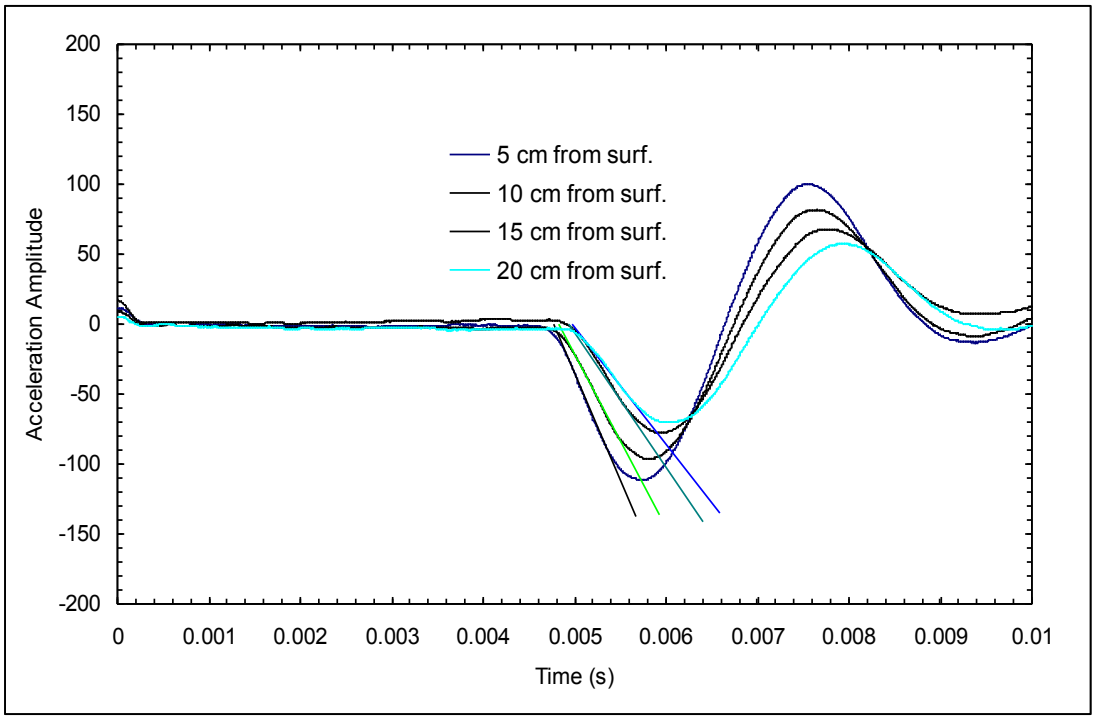

Fig. A.3. Elastic wave propagation in RSG used for determining the first arrival time.

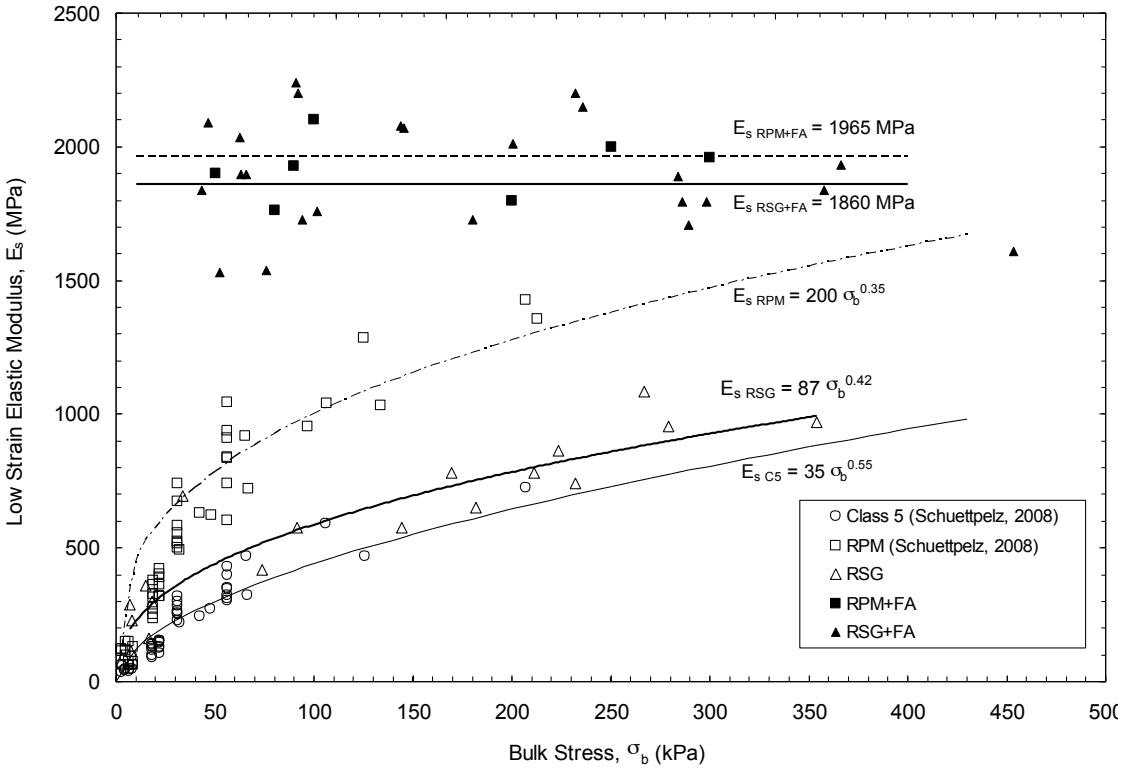

Fig. A.4. Low strain elastic modulus as a function of bulk stress.

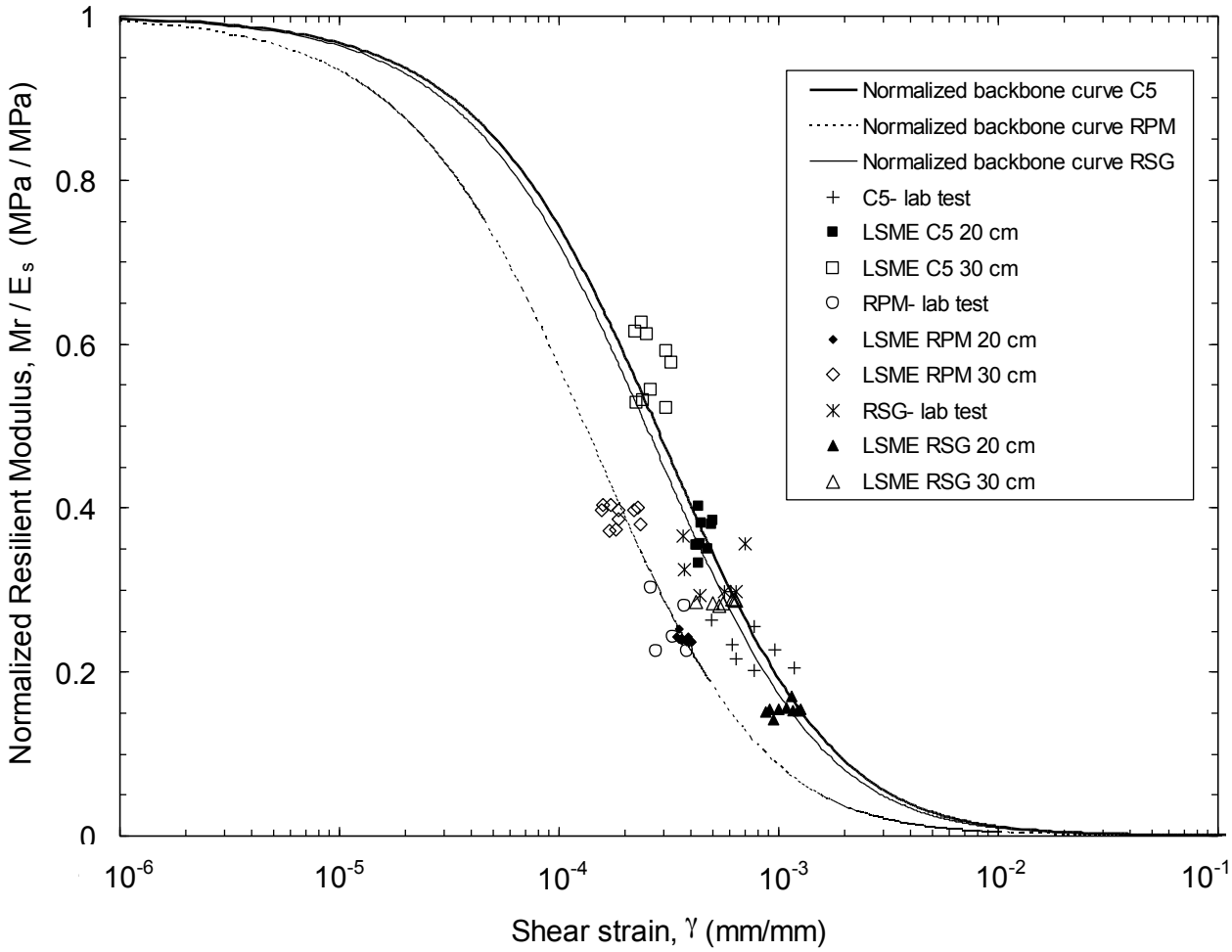

Fig. A.5. Backbone curve fit to LSME and laboratory data

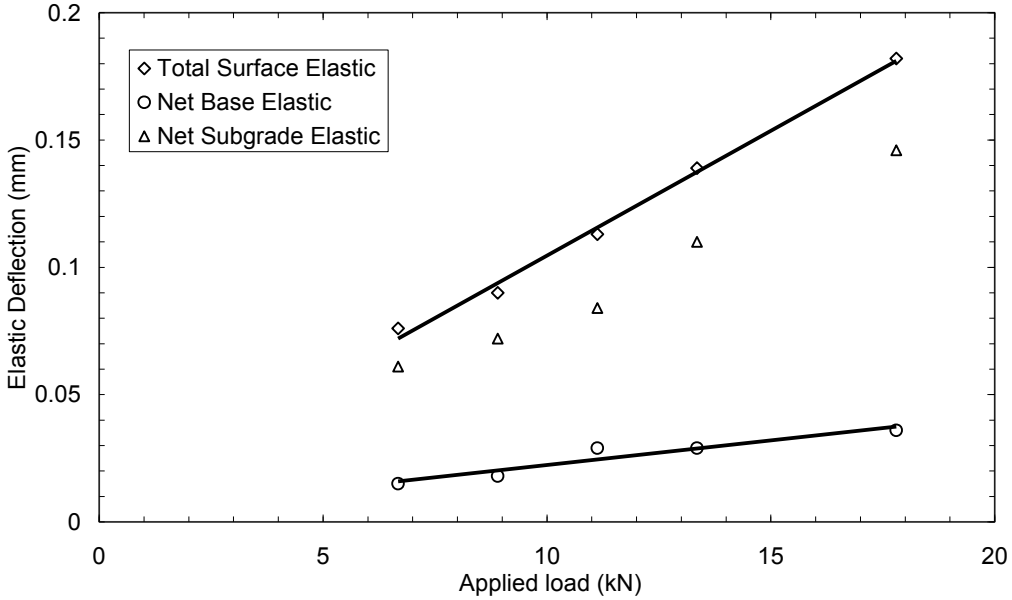

Fig. A.6. Evaluating the stress and strain dependency on modulus of stabilized RSG the LSME.

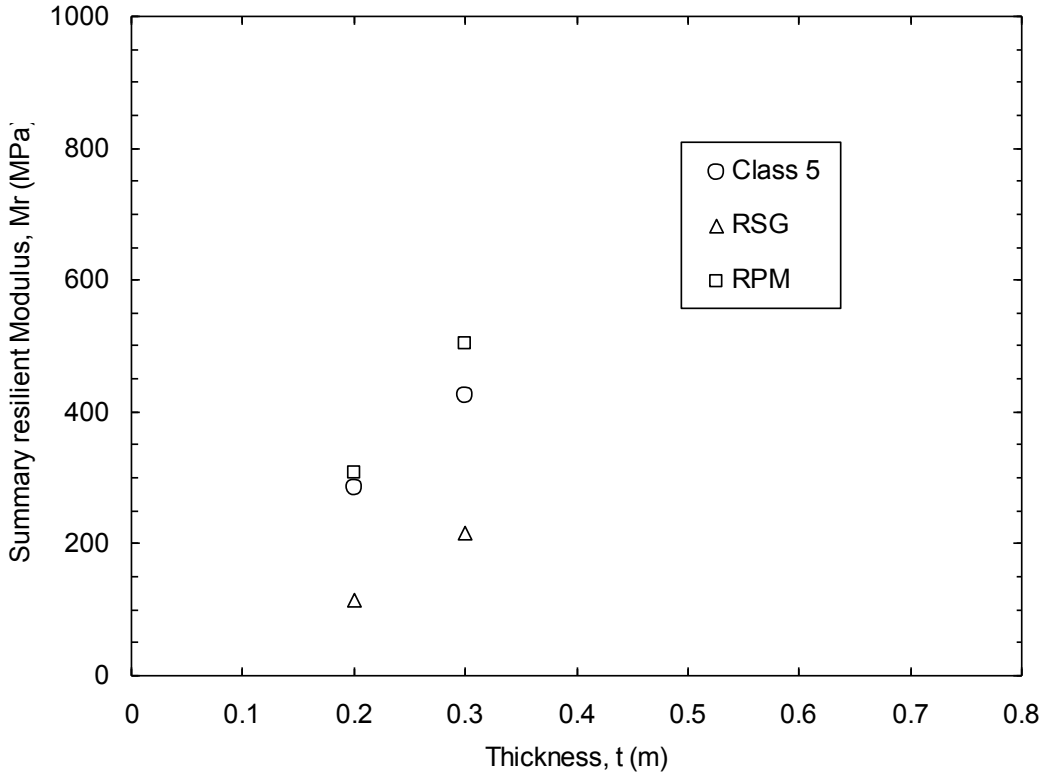

Fig. A.7. Summary resilient modulus as a function of base thickness in the LSME.

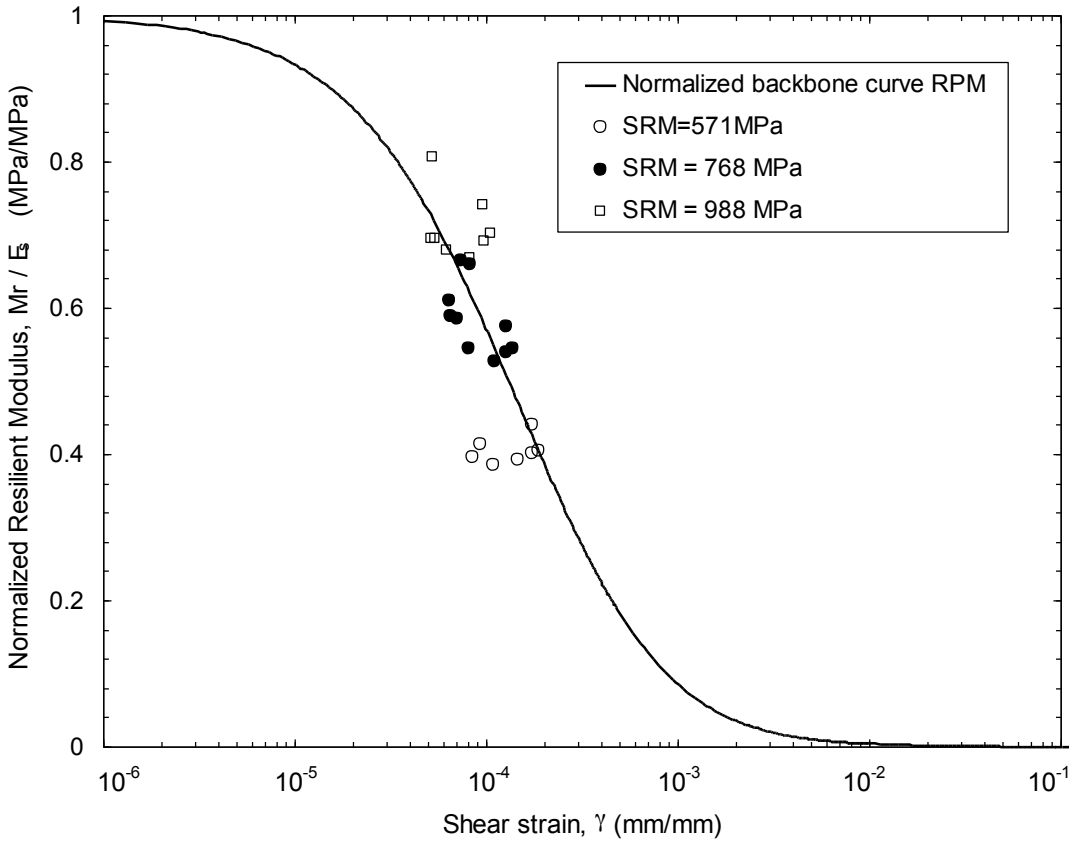

Fig. A.8. Various trials conducted to predict the summary resilient modulus for 0.45 m thick RPM.

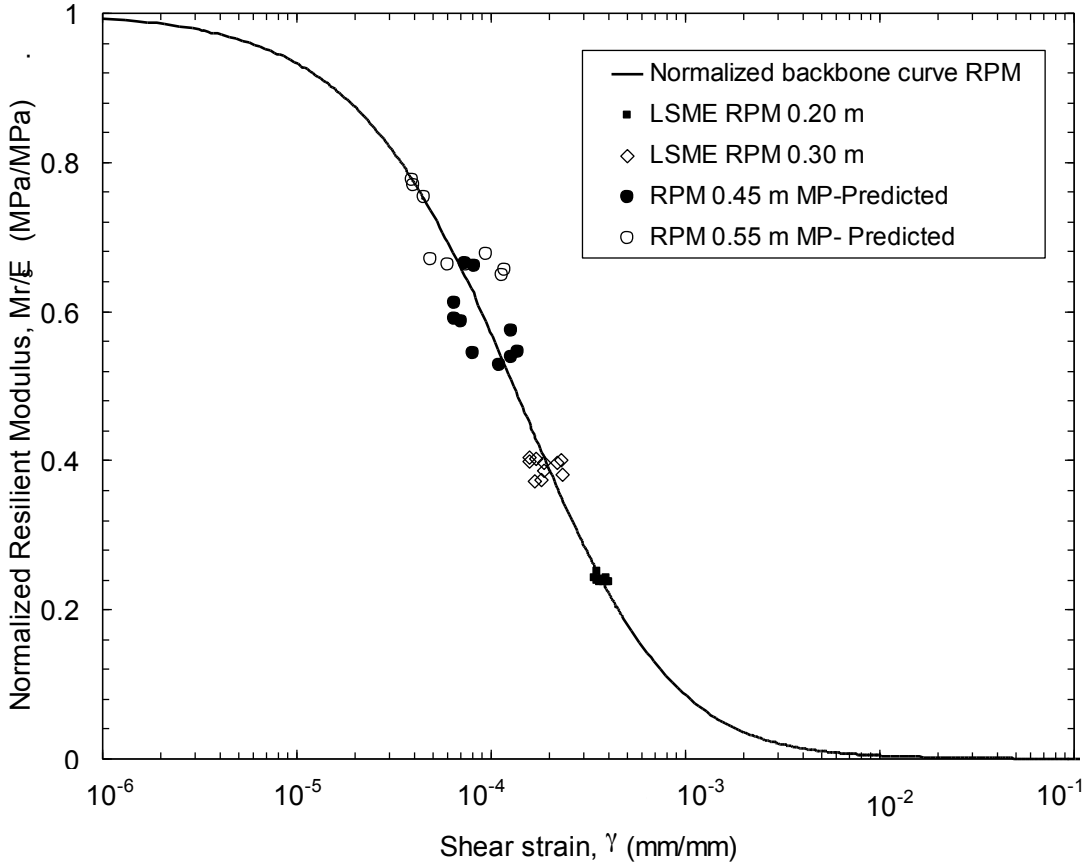

Fig. A.9. Prediction of summary resilient modulus with varying layer thickness of RPM.

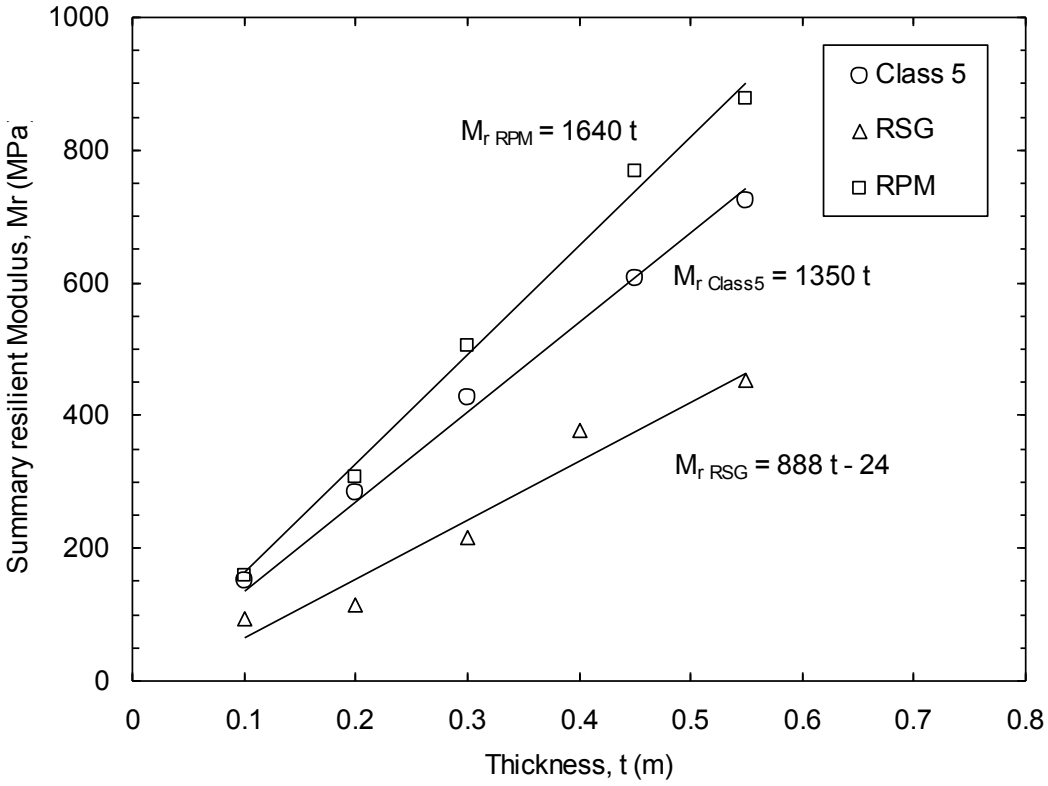

Fig. A.10. Summary resilient modulus as a function of thickness.

APPENDIX B: DETERMINATION OF LSME LOADING

The use of an asphalt concrete layer in the LSME was not considered practical for this study, so instead stress was applied directly to the base course surface. The stress applied to the base course surface of 133 kPa was selected from predictions computed by a pavement analysis software package called MICH-PAVE. This stress was applied with a steel plate having a radius equal to 12.7 cm. The purpose of this appendix is to explain how and why this stress and plate size was used in the LSME.

Stresses in a pavement profile were calculated using two different pavement analysis software programs: MICH-PAVE and KENLAYER. MICH-PAVE is a finite-element program using a grid and boundary conditions to perform calculations, while KENLAYER performs a layered system analysis. An analysis was performed with the base course modeled as both a linear elastic and a nonlinear elastic material with Eqn. 2.2. The output of the two programs is similar providing stresses, deflections and strains with depth and radial distance from the loading center.

The loading conditions and material properties required as inputs for the programs were determined from typical values either described by Huang (2003) or default values provided with the programs, and are listed in Table B.1. The stress applied to the asphalt surface was calculated from a single wheel load of 35.0 kN distributed over a circular area having a radius of 12.7 cm. The three-layer pavement profile consisted of 12.7 cm of asphalt concrete, over a 20.3 cm base layer, on top of a sandy subgrade.

The vertical stress as a function of depth into the pavement profile is graphed Figs. B.1a and B.1b resulting from MICH-PAVE and KENLAYER respectively. The curves from both programs have the same general shape, showing a sharp decrease in vertical stress in the asphalt concrete layer. The stress continues to decrease through the base layer, but at a slower rate than in the asphalt layer, and is relatively constant in the subgrade. MICH-PAVE and KENLAYER both show that when the base course is input

as a nonlinear elastic material, the stress at the base course surface is lower than with the linear analysis, but the stresses are similar at the subgrade surface.

The vertical stress on the surface of the base layer decreases with the radial distance from the loading center as shown in Fig. B.2a and B.2b as predicted by MICH-PAVE and KENLAYER respectively. Both programs show the greater stress resulting from the linear elastic base, which also decreases at a greater rate with the distance from the load center. MICH-PAVE computes slightly higher stresses than KENLAYER closer to the loading center, but these stresses also decrease at a steeper slope with the radial distance.

The stress from the nonlinear MICH-PAVE analysis was used in the LSME. The nonlinear behavior was considered to be more realistic of a granular material. Although KENLAYER and MICH-PAVE gave similar results, the finite-element method was considered to more accurately calculate mechanistic responses throughout the pavement profile due to a limited number of layers possible in KENLAYER.

The stress resulting from the steel plate used in the LSME was also modeled in the two programs and shown as Figs. B.1 and B.2. This stress appears as a rectangular area in Fig. B.2 because the stress is the same under the plate on the base course surface, and no stress is present adjacent to the plate. Although this is a different loading scenario than what is present when the stress is distributed through an asphalt layer, the selected plate size attempts to provide a best fit between applying the maximum stress on the base surface with the area of the base affected. The loading scenario used in the LSME results in the max stress applied to a greater area than what would be the case with asphalt present, so the loading is conservative. The stress from the plate decreasing with depth through the base layer is also shown in Fig. B.1, shifted to the right of the stresses from the asphalt layer.

Table B.1. Inputs used for MICH-PAVE and KENLAYER for determining stress on base layer.

Material Property or Load Condition	**Asphalt**	**Base**	**Subgrade**
Applied Load (kN)	35.0	6.7	NA*
Loading Radius (cm)	12.7	12.7	NA
Thickness (cm)	12.7	20.3	NA
Modulus (kPa)	3,275,000	398,000	48,000
K1, K2 (Eqn. 2.2)	NA	27,600 kPa 0.5	NA
Poisson's Ratio	0.35	0.35	0.45
Unit Weight (kN/m^3)	22.8	20.4	18.8

*NA = non-applicable

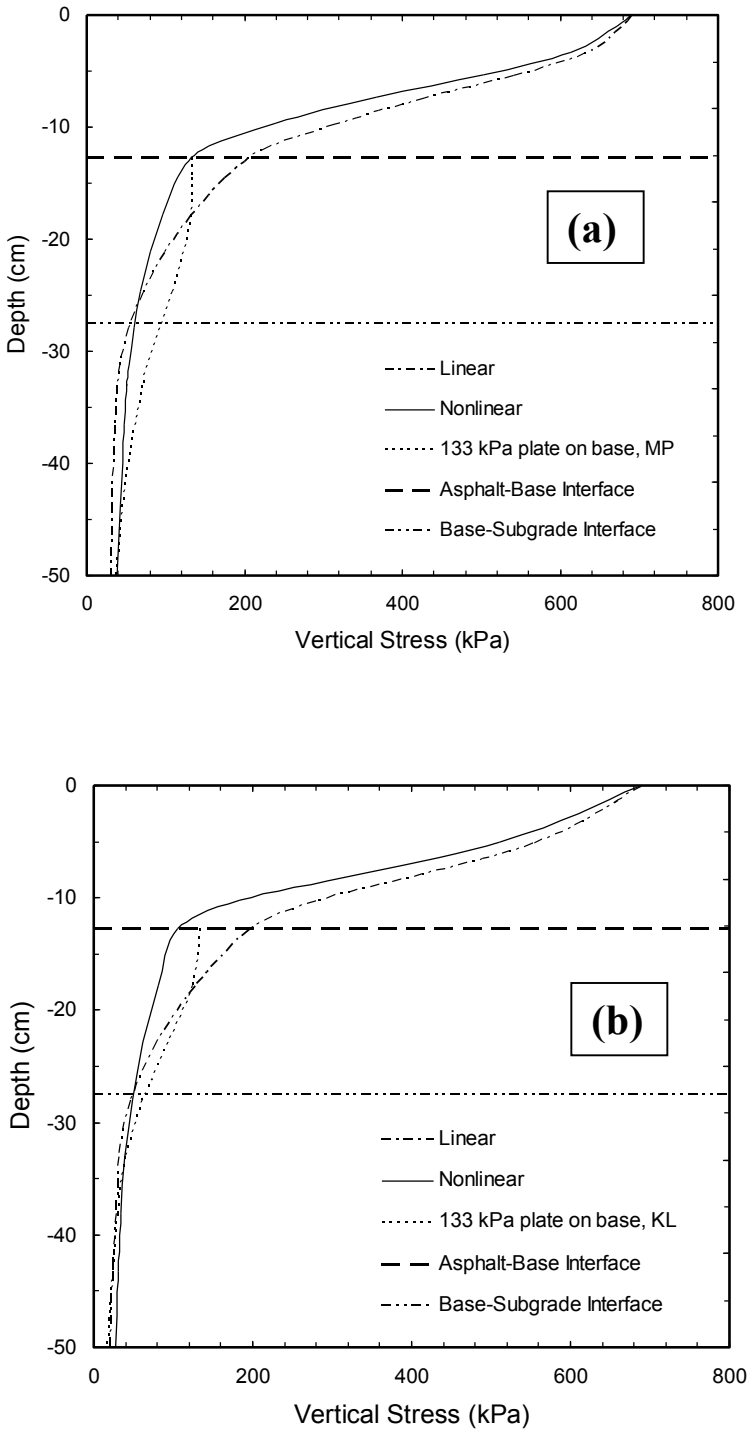

Fig. B.1. Prediction of vertical stress with depth resulting from traffic loading using (a) MICH-PAVE and (b) KENLAYER.

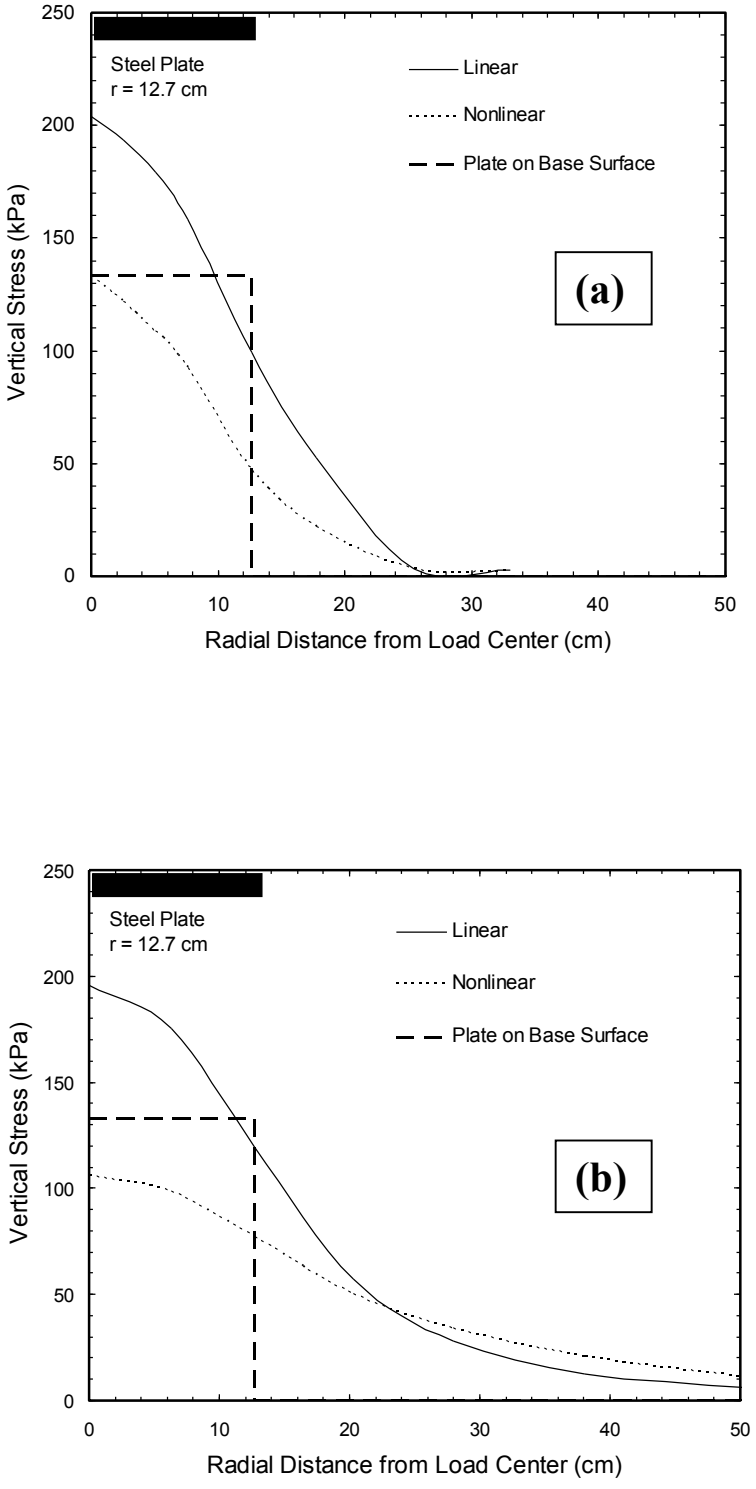

Fig. B.2. Prediction of vertical stress on base surface with radial distance resulting from traffic loading using (a) MICH-PAVE and (b) KENLAYER.

APPENDIX C: LSME SETUP AND LESSONS LEARNED

C.1. LSME SETUP AND OPERATION

The following step-by-step procedures were performed in setting up and conducting the LSME tests in this study.

C.1.1 LSME SETUP

1. Raise the steel beam above the test pit to the highest level possible using the overhead crane. Remove the loading plate and post from the hydraulic actuator. Place a sheet of plastic on the existing sand in the test pit to keep base materials separate.
2. Transport base material into the test pit using a skid loader. If blending a stabilizing material such as cement with the base, mix thoroughly with the skid loader on a flat section of pavement before placing in the test pit.
3. Compact the base material in the test pit at each desired lift thickness to maximum dry density at the optimum water content. A gas-powered jumping jack style compactor was used. Measure the density and water content of the compacted material with a nuclear density gage.
4. Drill or auger holes to the subgrade surface where deflections will be measured. For stabilized materials, holes should be drilled after compacting each lift and filled with plastic or another material that can be easily removed from the hole before placing an overlying lift.
5. Place the plate connected to the rod and tube on the subgrade surface at the bottom of the hole with the rod and tube coming up several cm above the base course surface. Precise placement of the rod coming up through the hole of the loading plate is required. Fill in the holes with base course material, compacting by hand around the rod and tube.
6. Ensure the area directly under the loading plate is smooth and level.

7. Attach the loading plate and post back onto the actuator. Lower the beam to the desired level, using caution while lowering the plate over the subgrade rod. Ensure the loading plate is not fully extended downward as the beam is lowered by raising it with the hydraulic actuator. Tighten all bolts securely when the beam is at the desired height.
8. Attach plates to the tops of the subgrade rods for LVDT measuring surfaces.
9. Place the LVDTs at desired locations, either on the loading plate, the base course surface, or the plates on the subgrade rods. Two LVDTS were mounted on opposite sides of the loading plate and averaged. Place a sheet of plastic over the test pit to prevent the material from drying out.

C.1.2 LSME OPERATION

1. Before turning on the hydraulic pressure, ensure the computer is turned on and that no LVDTs or other obstructions are directly above the plate, in case the plate moves upward.
2. Turn on the hydraulic pressure using the MTS controls adjacent to the test pit. Adjust the contact load applied by the plate using the MTS controls, and monitoring the load output with LABVIEW (or other program collecting data) on the computer.
3. Once the contact load is set, the LVDTs located on and/or above the loading plate can be moved into position.
4. Run the computer program for the desired number of cycles at the desired load.
5. After the test is completed, first remove the LVDTs above the plate before turning off the hydraulic pressure and computer.

C.1. LESSONS LEARNED REGARDING LSME TESTING

The following lessons learned during the LSME testing include suggestions and advice intended as a reference for conducting future tests in the LSME, and may save considerable time and effort.

1. Use the appropriate type of position transducers for measuring deflections. Deflection measurements were originally attempted with string-pot transducers where a cable is extended, but the deflections were too small to be accurately measured for the backcalculation of resilient modulus. Eventually LVDTs that could measure displacements to 0.005 mm were used effectively. If larger deflections are expected which exceed the travel distance of the LVDTs, the string-pot models may be more appropriate.
2. Position transducers must be properly calibrated. LVDTs were calibrated with the use of a micrometer mounted on a wooden frame.
3. Do not attempt to adjust the load or position of the steel plate while LVDTs or other objects are located in its path. The actuator controls are very sensitive, and a small turn of the control knob can result in sudden movement of the loading plate, damaging anything above or below it. Restarting the computer while applying a load may also cause movement of the plate, so LVDTs should only be mounted on or above the plate after setting the desired contact load, and then immediately removed before shutting off any equipment.
4. LVDTs should be mounted on a frame that is separate from the beam that the hydraulic actuator is mounted on. During cyclic loading, the beam experiences a displacement that will cause considerable noise in the LVDT measurements. Steel C-channels were placed on the concrete floor, creating a stable frame on which to mount the LVDTS (Fig. C.1).

5. The surface of the base course should be covered between placing the material in the test pit and running the test. The stiffness of the material is dependent on the moisture content, and smaller deflections will be measured as drying of the material occurs.
6. Stabilized material was removed from the test pit with an electric breaker rented from a local hardware store.

Fig. C.1. Mounting LVDTs on C-channel frame.